Annual Report April 1, 2010 - March 31, 2011

UTTAC-80, 2012

UTTAC

ANNUAL REPORT 2010

TANDEM ACCELERATOR COMPLEX
Research Facility Center for Science and Technology
University of Tsukuba

http://www.tac.tsukuba.ac.jp/

UTTAC

ANNUAL REPORT 2010

April 1, 2010 – March 31, 2011

UTTAC-80 2012

Executive Editor: Eiji Kita
Editors: Yoshihiro Yamato, Daiichiro Sekiba, Kimikazu Sasa, and Tetsuro Komatsubara

---

UTTAC is a series of issues, which include annual reports of
Tandem Accelerator Complex, Research Facility Center
for Science and Technology, University of Tsukuba.
The issues may also include irregular reports written by English.

Tandem Accelerator Complex, Research Facility Center for Science and Technology,
University of Tsukuba
Tennodai 1-1-1, Tsukuba, Ibaraki 305-8577, Japan

http://www.tac.tsukuba.ac.jp/
annual@tac.tsukuba.ac.jp

PREFACE

This annual report covers researches carried out at University of Tsukuba Tandem Accelerator Complex (UTTAC) during the fiscal year 2010 (1 April 2010 ~ 31 March 2011). The topics include not only accelerator-based researches using the 12UD Pelletron and 1 MV Tandetron accelerators, but also closely related researches to UTTAC including Mössbauer experiments.

On 11 March 2011, the Great East Japan Earthquake struck east part of Japan with subsequent tsunami. The fierce quake of 9.0-magnitude and the tsunami wave of 10 m high killed more than 15,000 people in Iwate, Miyagi, Fukushima prefectures. About 3500 people are still missing. Nuclear plants in Fukushima were seriously damaged resulting to leak radioactive material. The strong shock of the earthquake also hit our tandem accelerator at Tsukuba. However no casualty in our laboratory, the tank of the 12 UD Pelletron accelerator was shaken and the structure of terminal and column was collapsed completely. Three ion sources at the ninth floor were broken. At this moment we are planning to build new accelerator in the 2nd experimental room and to connect the beam line to facilities in the 1st experimental room. This report includes the damage of our experimental facilities.

10 January, 2012

Editors

CONTENTS

1.

ACCELERATOR AND EXPERIMENTAL FACILITIES

1.1 Accelerator operation (2010)

K. Sasa, S. Ishii, H. Kimura, H. Oshima, Y. Tajima, T. Takahashi, Y. Yamato,
T. Komatsubara, D. Sekiba and E. Kita.

The University of Tsukuba, Tandem Accelerator Complex (UTTAC) has two accelerators, the 12UD Pelletron tandem accelerator and the 1 MV Tandetron accelerator. The total service time of the UTTAC multi-tandem accelerator facility was 125 days (3,000 hours) in the fiscal year 2010. 24.8 % (744 hours) of the total service time was used for industrial users, under the project "Promotion of Advanced R&D Facility Utilization", which was supported financially by the Ministry of Education, Culture, Sports, Science and Technology (MEXT) of JAPAN.

1.1.1 The 12UD Pelletron tandem accelerator

The operating time and the experimental beam time of the 12UD Pelletron tandem accelerator were 2040.3 and 1603.1 hours, respectively, during the fiscal year 2010. Fig.1 shows the accelerator operation hours per month. Fig.2 shows the beam time histogram with respect to the terminal voltage. Fig.3 represents the percentage of the operation hours for the three ion sources and ion species.

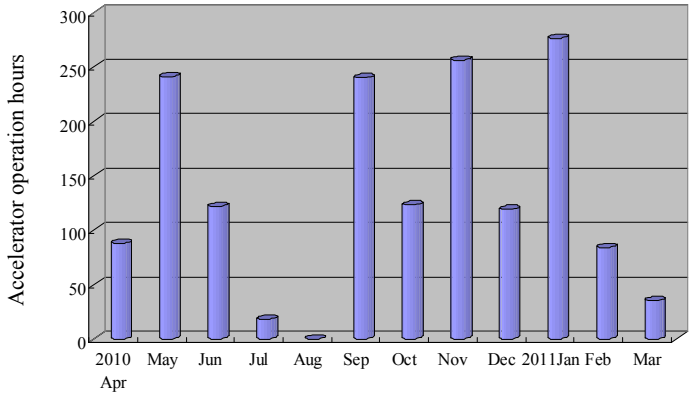

Fig.1. Accelerator operation hours per month for the 12UD Pelletron tandem accelerator in 2010.

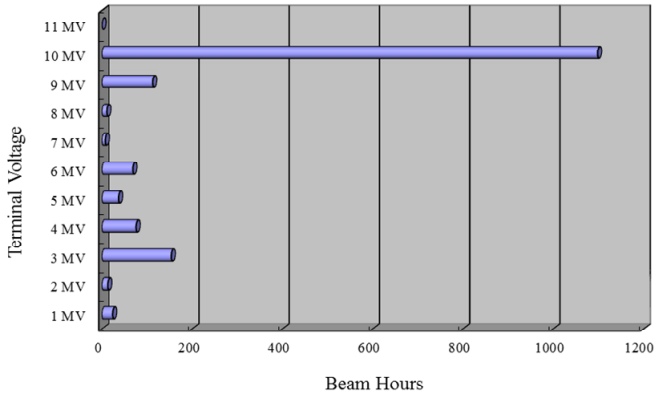

Fig.2. Beam time histogram as a function of the terminal voltage for the 12UD Pelletron tandem accelerator in 2010.

The periodic maintenance of the 12UD Pelletron tandem accelerator was scheduled for the spring of 2010, but was postponed on July due to the breakdown of a SF_6 gas-recovery unit. The maintenance in the accelerator tank was performed during the summer period.

In 2010, a total of 65 research programs were carried out using the 12UD Pelletron tandem accelerator. A total of 694 researchers used the 12UD Pelletron tandem accelerator. Fig.4 shows the percentage of the experimental beam time for the running research fields with the 12UD Pelletron tandem accelerator.

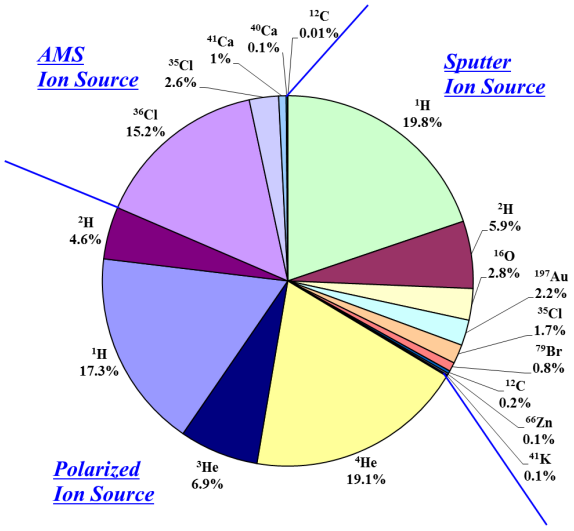

Fig.3. Percentage of the operation hours for the three ion sources and ion species in 2010.

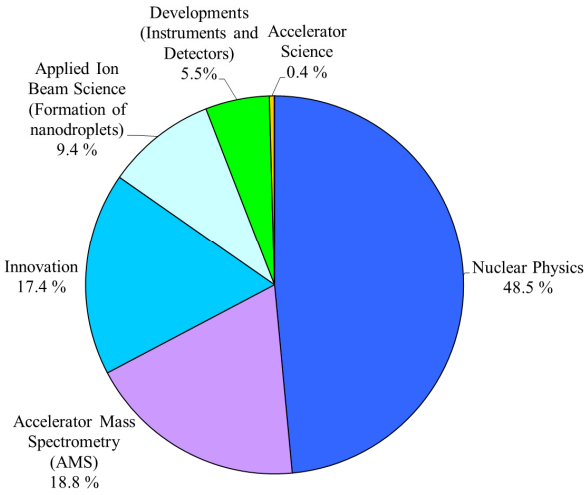

Fig.4. Percentage of the experimental beam time for the running research fields in 2010.

1.1.2 The 1 MV Tandetron accelerator

The operating time and the experimental beam time of the 1MV Tandetron accelerator were 553.3 and 235 hours, respectively, during the total service time in 2010. A total of 37 research programs were carried out and a total of 256 researchers used the 1 MV Tandetron accelerator. Fig. 5 shows the percentage of accelerated ions for the 1 MV Tandetron accelerator. Fig. 6 shows the percentage of the experimental beam time for the running research fields. The main applications in the use of the 1 MV Tandetron accelerator are PIXE, RBS/ERDA, NRA and cluster physics.

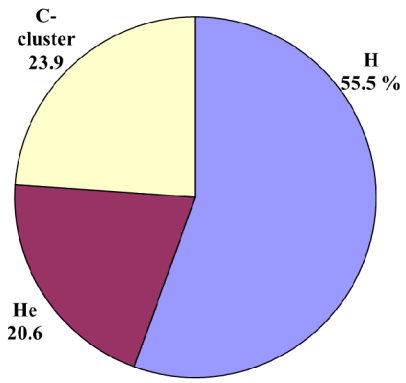

Fig.5. Percentage of accelerated ions for the 1 MV Tandetron accelerator in 2010.

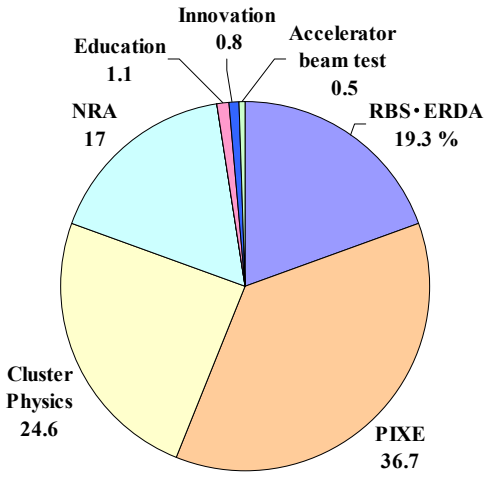

Fig.6. Percentage of the experimental beam time for the running research fields with the 1 MV Tandetron accelerator in 2010.

1.1.3 Damage Situation of the 12UD Pelletron tandem accelerator by the Great East Japan Earthquake

By the Great East Japan Earthquake on 11 March 2011, the 12UD Pelletron tandem accelerator suffered serious damages. On the day, 12UD Pelletron tandem accelerator was in operation at 8 MV for ^{41}Ca trial measurements by AMS. The electricity supply went out during the earthquake. The blackout lasted for 4 days, and we had to stop the electric power to our facility for 2 days in a row for hazard avoidance. We could not access our facility for the first week because of many aftershocks. Fortunately, there were no casualties by this earthquake in the facility. The 1 MV Tandetron accelerator did not have any serious damage because of its T type hard structure and it has worked properly after the earthquake. Fig. 7 shows a summarized damage situation at the UTTAC caused by the Great East Japan Earthquake.

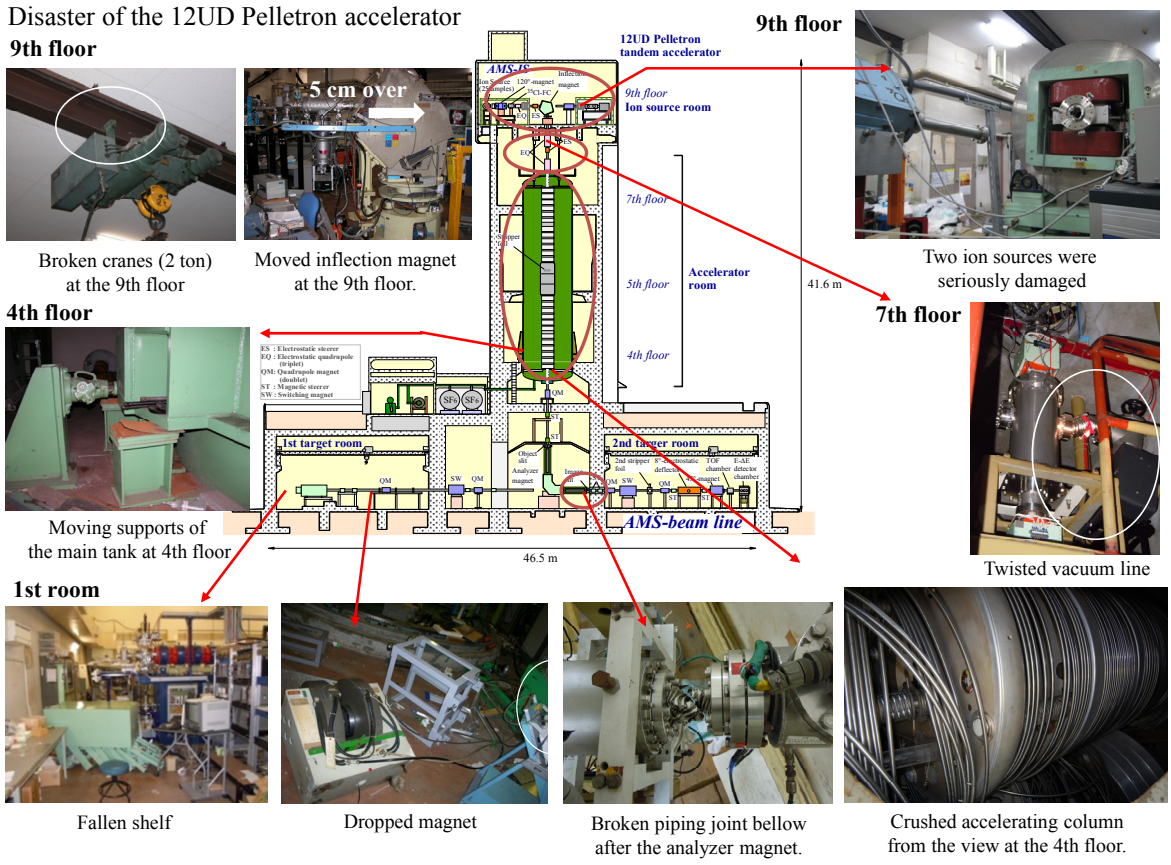

Fig. 7. A summarized damage of the 12UD Pelletron tandem accelerator.

Ion sources at the 9th floor

Two of three ion sources at the 9th floor were also seriously damaged by the earthquake. The anchor bolts of the Wien filter for the polarized ion source were destroyed by the earthquake. Finally, the Wien filter was moved one meter from the beam line by the earthquake and aftershocks (Fig. 8). Almost piping bellows between connected heavy loads were broken by shaking. Ceramic columns of the AMS ion source were also broken (Fig. 9). Water pressure gauges of the cooling water system were shaken and broken off by its root on the plumbing. A water spurt came out the polarized ion source (Fig. 10). The inflection magnet at the 9th floor was moved 5 cm on the mount by the earthquake as shown in Fig. 11.

Fig.8 Photo of the Wien filter moved from the beam line caused by the earthquake.

Fig.9 Photo of the broken ceramic columns for the AMS ion source.

Fig.10 The flooded polarized ion source due to the broken water pressure gauges of the cooling water system.

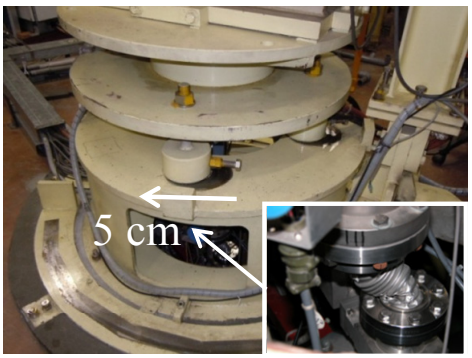

Fig.11 Photo of the moved inflection magnet.

Main accelerator

A main tank of the 12 UD Pelletron tandem accelerator located from downstairs 4th floor to 7th floor was strongly shaken by the shock of the earthquake. Three shock prevention devices for the accelerator tank at the 7th floor were pushed out with breaking anchor bolts of 1 inch in diameter as shown in Fig. 12. Weight supports and jacks at the 4th floor were moved as nearly taken off as shown in Fig. 13. All high voltage accelerating columns fell down in the accelerator tank (Fig. 14). Fig. 15 shows the downed accelerating column in the tank at the bottom. Structures of terminal shell and columns inside the tank were completely collapsed.

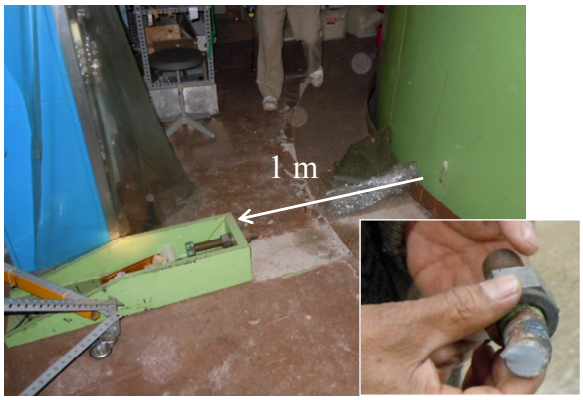

Fig.12 Photo of the moved shock prevention devices at the 7th floor.

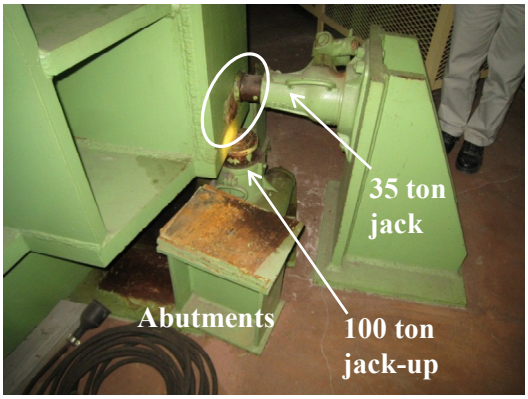

Fig.13 Photo of the moved weight supports and jacks at the 4th floor.

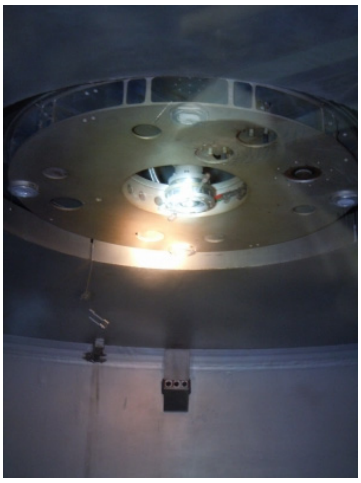

Fig.14 Lost columns inside of the tank observed from a manhole at 7th floor.

Fig.15 Photo of the fallen terminal shell and accelerator columns at the tank bottom.

At the 1st floor, a NMR experimental magnet was dropped with breaking a stepladder as shown in Fig. 7. Several tool racks also fell down in the facility. Many magnets were moved and a number of joint bellows were broken as shown in Fig. 16. A shielding door motor was broken by the shock of the earthquake at the analyzer magnet room (Fig. 17). Therefore, we could not access immediately in the analyzer magnet room after the earthquake. Shielding concrete blocks at the analyzer magnet room came down to the floor as shown in Fig. 18.

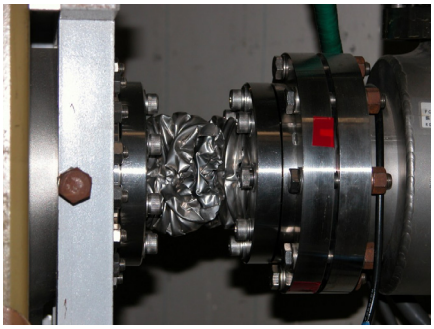

Fig.16 Broken joint bellows at the 1st floor.

Fig.17 Broken shielding door motor at the analyzer magnet room.

Fig.18 Fallen shielding concrete blocks at the analyzer magnet room.

Earthquake disaster reconstruction project

We decided to shut down the 12UD Pelletron tandem accelerator in 2011. At present, the UTTAC tries to install a new middle-sized tandem accelerator instead of the broken 12UD Pelletron tandem accelerator since it is difficult to repair the previous one due to some boundaries in the building construction. We have a plan to install the new accelerator system at the 2nd target room connecting the beam line to the present experimental facilities at the 1st target room. The construction of the new accelerator system is scheduled in the spring of 2014.

1.2 Status of the Tsukuba AMS system (2010)

K. Sasa, T. Takahashi, K. Sueki, N. Kinoshita, T. Amano, J. Kitagawa, K. Kurosumi, M. Matsumura, S. Abe, T. Nishimura, Ying-Shee Wong, Y. Matsushi[1], Y. Tosaki[2], K. Bessho[3], H. Matsumura[3]

A multi-nuclide AMS system on the 12UD Pelletron tandem accelerator at the University of Tsukuba (Tsukuba AMS system) can measure environmental levels of long-lived radioisotopes of ^{14}C, ^{26}Al, ^{36}Cl and ^{129}I by employing a molecular pilot beam[1]. The high terminal voltage has an advantage in the detection of heavy radioisotopes. The Tsukuba AMS research group has focused its activities on ^{36}Cl measurements. In 2010, a total of 242 samples for ^{36}Cl were measured by the Tsukuba AMS system, and total operation time was 43 days. Currently, a total of 8 research projects for earth and environmental sciences have been conducting by the Tsukuba AMS system. Table 1 shows current research programs and the number of samples in 2010. We have measured cosmogenic ^{36}Cl in the Dome Fuji ice core, Antarctica and the NEEM ice core, Greenland. They are expected to provide bipolar information for the paleo-environmental reconstruction. We also investigate attenuation of muons and production rates of long-lived isotopes relevant to underground environment. We have performed the environmental monitoring for nuclear facilities to detect long-lived radioisotopes by AMS.

A first international ^{36}Cl interlaboratory comparison has been initiated. Evaluation of the final results of the eight participating AMS laboratories on three synthetic AgCl samples shows no difference in the sense of simple statistical significance [2].

Table 1 Research programs and the number of samples by the Tsukuba AMS system in 2010.

AMS research programs	Target material	Organization	Number
^{36}Cl-AMS ^{36}Cl in the ice cores.	Ice core	Univ. of Tsukuba	73
Measurement of ^{36}Cl in soil. Environmental monitoring for nuclear facilities by AMS.	Soil	Univ. of Tsukuba	58
Bomb-produced ^{36}Cl as a tracer in groundwater.	Hydrological samples (ground water, rain water)	AIST	70
In-situ ^{36}Cl for denudation rates of karst landform. ^{36}Cl exposure dating for Tiankeng.	Limestone	Kyoto Univ. Univ. of Tsukuba	21
Production rates of ^{36}Cl for target elements in chondritic meteorites.	Meteorite	Tokyo Metro. Univ.	14
^{36}Cl produced in muon irradiation.	NaCl, $CaCO_3$	Univ. of Tsukuba	2
^{36}Cl in natural magnetite.	Magnetite	Univ. of Tsukuba KEK	4
^{41}Ca-AMS ^{41}Ca-AMS development.	CaF_2	Univ. of Tsukuba	20

[1] Disaster Prevention Research Institute, Kyoto University
[2] Geological Survey of Japan, National Institute of Advanced Industrial Science and Technology (AIST)
[3] Radiation Science Center, High Energy Accelerator Research Organization (KEK)

^{41}Ca AMS

^{41}Ca-AMS has been developed by modifying the current AMS system at the UTTAC. We have performed trial measurements at 8 MV to accelerate $^{41}CaF_3^-$ with a pilot beam of $^{66}ZnO_2^-$. We use CaF_2 mixed with ZnO and Ag as a target material. Fig. 1 shows a schematic layout of ^{41}Ca AMS. $^{41}Ca^{5+}$ ion with 43.35 MeV is measured by a gas ΔE – SSD E detector. Fig. 2 shows an estimation of the energy loss in the detector. We expect that ^{41}Ca can be separated clearly from isobaric interference of ^{41}K by this AMS techniques.

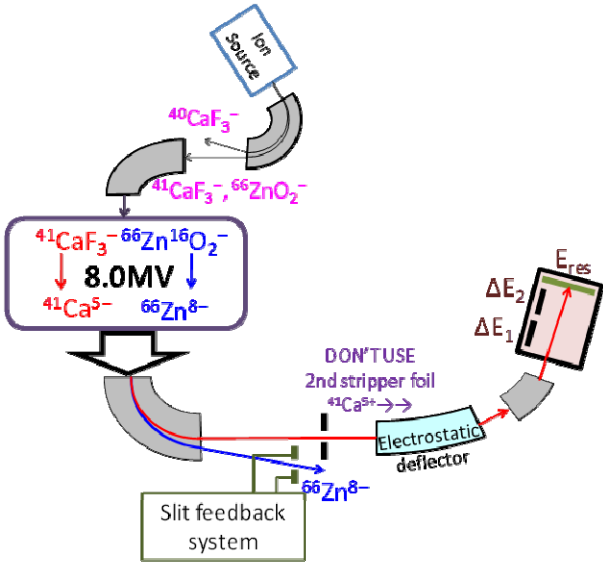

Fig.1 Schematic layout of ^{41}Ca AMS at UTTAC.

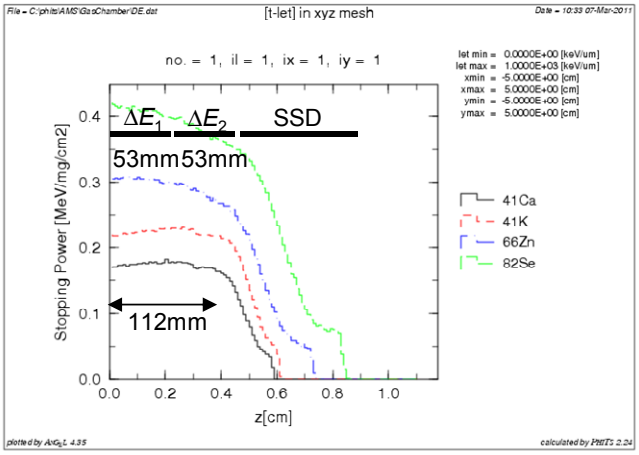

Fig. 2 Estimation of the energy loss in the gas ΔE – SSD E detector.

Acknolagements

This work is supported in part by the Grants-in-Aid for Scientific Research Programs of the Ministry of Education, Culture, Sports, Science and Technology, Japan (Grants-in-Aid No. 21310004, 22241003 and 23656586) and Pre-Strategic Initiatives (Research Base-Building), the University of Tsukuba.

References

[1] K. Sasa et al., , *Nucl. Instr. and Meth. B* 268 (2010) 1193-1196.

[2] S Merchel et al., Ultra-trace analysis of ^{36}Cl by accelerator mass spectrometry: an interlaboratory study, *Analytical and Bioanalytical Chemistry*, 400 (2011) 3125-3132.

2.

NUCLEAR PHYSICS

2.1 Study of the structure of ^{30}S by in-beam gamma ray spectroscopy and the ^{29}P(p,γ)^{30}S reaction rate in classical novae phase II

K. Setoodehnia*, A. A. Chen*, T. Komatsubara‡, Y. Abe‡, J. Chen*, S. Cherubini†,♯, S. Fukuoka‡, Y. Ishibashi‡, Y. Ito‡, S. Kubono%, D. Kahl%, T. Moriguchi‡, K. Okumura‡, H. Ooishi‡, A. Ozawa‡, S. Nakamura‡, D. Nagae‡, R. Nishikiori‡, T. Niwa‡, H. Suzuki‡, K. Yokoyama‡, T. Yuasa‡

* Department of Physics & Astronomy, McMaster University, Hamilton, ON L8S 4M1, Canada

‡ Institute of Physics, University of Tsukuba, Tennodai 1-1-1, Tsukuba, Ibaraki 305-8577, Japan

% Center for Nuclear Study (CNS), University of Tokyo, Wako Branch at RIKEN, 2-1 Hirosawa, Wako, Saitama, 351-0198, Japan

† Dipartimento di Fisica e Astronomia, Università di Catania, Catania, Italy

♯ Laboratori Nazionali del Sud-INFN, Catania, Italy

The thermonuclear ^{29}P$(p,\gamma)^{30}$S reaction rate is strongly dependent on the nuclear structure of ^{30}S states, and is important in two astrophysical scenarios, namely, classical novae and type I x-ray bursts. Both these astrophysical phenomena are very energetic stellar explosions powered by thermonuclear runaway as a result of explosive hydrogen burning on the surface of the compact object in close semi-detached binary systems, that consist of a white dwarf (in the case of classical novae) or a neutron star (in the case of x-ray bursts) and a low-mass companion star.

The ^{29}P$(p,\gamma)^{30}$S reaction rate at temperatures characteristics of explosive hydrogen burning in classical novae and x-ray bursts (0.1 – 1.5 GK) had been previously predicted [1] to be dominated by two low-lying, unobserved, levels in ^{30}S in the $E_x = 4.7 - 4.8$ MeV region, with spin and parity assignments of 3^+_1 and 2^+_3, respectively. In recent experimental work, two candidate levels were observed with energies of 4699(6) keV and 4814(3) keV, but no definitive experimental information on their spins and parities was obtained [2].

In 2009, an in-beam γ-ray spectroscopy study of ^{30}S with the ^{28}Si(^{3}He, $n\gamma$)^{30}S reaction was performed at UTTAC in order to construct the decay schemes of proton-unbound states in ^{30}S with a γ-γ coincidence analysis of their decay γ-rays [3].

Among the ^{30}S levels observed in that experiment, three were above the proton threshold, including two levels at 4810.4(6) keV and 4688.0(4) keV [4], which correspond to the two astrophysically important states predicted by Iliadis *et al.* [1]. The reconstructed energies for these two levels are in agreement with the results of an earlier particle transfer measurement [2]. One γ-ray was also observed at 845.5(2) keV, the origin of which is still under investigation.

In order to infer or constrain the spin-parity assignments of these two states, phase II of the in-beam γ-ray spectroscopy measurement was performed at UTTAC during September 2010. A 9 MeV ^{3}He beam impinged on a natural Si target of 25 μm thickness. In order to measure the Directional Correlation of Oriented (DCO) nuclei ratios of the relevant transitions, γ-γ coincidence measurements were performed with two high purity Ge-detectors with relative efficiencies of 70% and 50%, placed at 135° and 90° with respect to the beam axis, respectively.

The relative intensities and decay branches of all the observed transitions at 90° and 135° were obtained. In particular, the decay branches of the two astrophysically important states at 90° were compared to the known branches of the potential mirror state candidates in ^{30}Si, also measured at 90° [5]. The branching ratios of the respective γ-transitions of these two states were in agreement with those of the ^{30}Si mirror levels [5]. This experimental evidence strongly suggested that the spin-parity assignments for these two states have been correctly assumed in the previous measurement [2].

In addition, the DCO ratios were obtained only for the strongly populated γ-rays of ^{30}S. The DCO ratios are defined as $R = I^{\gamma_2}_{\theta_1}$ (Gate $I^{\gamma_1}_{\theta_2}$)/$I^{\gamma_2}_{\theta_2}$ (Gate $I^{\gamma_1}_{\theta_1}$), where $\theta_1 = 135°$ and $\theta_2 = 90°$, and the gated transition was γ_1: $2^+_1 \rightarrow 0^+_1$ transition. The decay branches of the 4810.4(6) keV state to the first and second excited states in ^{30}S were observed at 90°; however, these branches were very weak at 135°. Therefore, no DCO ratios for these transitions could be determined, and thus the spin-parity of this state remains tentatively assigned as (2^+_3). The proposed 3^+_1 state decays to the 2^+_1 state emitting a γ-ray with an energy of 2477.1(2) keV. An experimental DCO ratio of 0.37 ± 0.04 was determined for this transition. The theoretical DCO ratio for this transition is determined to be 0.5 under the assumption that it is a pure dipole. The discrepancy between the experimental and the theoretical DCO ratio for this transition, indicates that it is a mixed $M1$, $E2$ transition. The mixing ratio could not be determined for this transition.

Angular distributions of the lowest lying γ-rays of ^{30}S were also measured with the 70% efficiency detector located at 135°, 120°, 110°, 100° and 90°, while the 50% efficiency detector was fixed at 90°. The γ-ray corresponding to the $2^+_1 \rightarrow 0^+_1$ transition is a pure $E2$ transition, as expected. An experimental value of $\sigma/J = 0.55$, as well as $\frac{A_2}{A_0} = 0.40 \pm 0.20$ and $\frac{A_4}{A_0}$ = -0.009 ± 0.180 were determined for this γ-ray transition. On the other hand, the γ-ray corresponding to the $2^+_2 \rightarrow 2^+_1$ transition is a mixed $M1$, $E2$ transition, for which an experimental $\frac{A_2}{A_0} = 0.38 \pm 0.25$ and $\frac{A_4}{A_0}$ = -0.14 ± 0.22, a value of $\sigma/J = 0.4$, and a mixing ratio of $\delta = 0.16 \pm 0.04$ were determined. The γ-rays from higher-lying states do not appear in the singles spectrum, and thus their angular distributions could not be determined.

References

[1] C. Iliadis, J. M. D'Auria, S. Starrfield, W. J. Thompson and M. Wiescher, Astrophys. J. Suppl. Ser. 134 151 (2001).

[2] K. Setoodehnia, A. A. Chen, J. Chen, J. A. Clark, C. M. Deibel *et al.*, Phys. Rev. C 82 022801(R) (2010).

[3] K. Setoodehnia, A. A. Chen, T. Komatsubara, Y. Sugiyama, A. Ozawa *et al.*, UTTAC Annual Report 2009, UTTAC-79 p. 9 (2010).

[4] K. Setoodehnia, A. A. Chen, T. Komatsubara, S. Kubono *et al.*, Phys. Rev. C 83 018803 (2011).

[5] D. E. Alburger and D. R. Goosman, Phys. Rev. C 9 2236 (1974).

2.2 Study of nuclearsynthesis of ^{26}Al by gamma ray spectroscopy IV

T. Komatsubara, T. Yuasa, T. Hayakawa*, S. Kubono#

* JAEA

CNS, Tokyo University

Since observation of 1.809-MeV gamma rays by satellite gamma ray telescope has been reported[1], the astrophysical study of ^{26}Al is very important for nuclear synthesis. Observed mass ratio between ^{26}Al and ^{60}Fe of 0.11±0.03 by INTEGRAL[2] is rather small than the calculated ratio[3].

The nucleus ^{26}Al can be created by ^{24}Mg(p,γ)^{25}Al(β^+,ν)^{25}Mg(p,γ)^{26}Al reaction. The ground state of ^{26}Al, which is 5^+ and 0.72 m year of half life, feeds 2^+ of ^{26}Mg emitting the gamma ray of 1.809-MeV. However there is a bypass reaction sequence of ^{24}Mg(p, γ)^{25}Al(p,γ)^{26}Si(β^+,ν)^{26m}Al(β^+,ν)^{26}Mg reaction which feed the ground state of ^{26}Mg directly without 1.809-MeV gamma ray emission. In order to reproduce stellar abundance of the ^{26}Al the investigation of the excited states of ^{26}Si is important for the evaluation of the bypass reaction rate. There several studies for the excited states above proton threshold by using reaction mechanism[4-7] and gamma ray spectroscopy[8]. In our previous studies, one new level is found at 5886-keV in the ^{26}Si[9]. We assigned spin of the state as 0^+ by gamma-ray angular correlation measurements[10].

Through the angular correlation measurement there are uncertainties about spin alignments of the initial states emitting gamma rays. In order to estimate the alignments of nuclear orientation a gamma ray angular distribution measurement was carried out at UTTAC. The excited states of ^{26}Si were populated by the nuclear reaction ^{24}Mg(^{3}*He*, *n*)^{26}Si. The ^{3}He beam of 10 MeV was irradiated on a natural Mg target. Target thickness of the Mg foil is 3 mg/cm^2. Gamma ray single spectrum was measured at the angle of 90°, 100°, 110°, 120°, 130° and 140° by using Ge detector of 70% efficiency at 1333-keV. The yields of the gamma rays were normalized by the yield of $2_1^+ \rightarrow 0^+$ transition of ^{26}Si measured by another monitor detector of 50% efficiency located at 90°.

In Fig. 1 the measured angular distribution of the $2_1^+ \rightarrow 0^+$ transition of ^{26}Si is shown as $W(\theta)/W_0$ where the normalization factor W_0 is deduced by assuming distribution of $W(\theta)=W_0(1+A_2P_2\cos(\theta)+A_4P_4\cos(\theta))$. The observed distribution is very disturbed from stretched E2 transition having A_2=0.71 and A_4=-1.71. In the Fig 1 expected distributions are shown by a solid line for σ/J = 0.5 and by a dashed line for σ/J =1. In Fig 2, the distribution of $2_2^+ \rightarrow 2_1^+$ is shown with the estimated distributions of solid and dashed lines with σ/J = 0.5 and 1, respectively. Mixing ration of $\langle||E2||\rangle/\langle||M1||\rangle$ are taken to be 0.21 from reference[11]. Both observed gamma ray distributions are strongly depressed as the σ/J factor should be 1 or larger. The reason of the distortion could arise by emission of neutrons and gamma rays, and unexpected strong perturbations. The large distribution parameters of the initial alignment σ/J being 1 or larger are consistent to our previous analysis of DCO ratios.

References

[1] R. Diehl, H. Halloin, K. Kretschmer, G.G. Lichti, V. Schönfelder, A.W. Strong, A. Kienlin, W. Wang, P. Jean, J. Knödlseder, J.P. Roques, G. Weidenspointner, S. Schanne, D.H. Hartmann, C. Winkler, C. Wunderer, Nature 439 (2006) 45.

[2] M.J. Harris, et al., Astron Astrophys 433 (2005) L49

[3] S.E. Woosley, A. Heger, Physics Report 442 (2007) 269

[4] D.W. Bardayan, J.C. Blackmon, A.E. Champagne, A.K. Dummer, T. Davinson, U. Greife, D. Hill, C. Iliadis, B.A. Johnson, R.L. Kozub, C.S. Lee, M.S. Smith, P.J. Woods, Phys. Rev. C 65 (2002) 032801(R).

[5] J.A. Caggiano, W.B. Smith, R. Lewis, P.D. Parker, D.W. Visser, J.P. Greene, K.E. Rehm, D.W. Bardayan, A.E. Champagne, Phys. Rev. C 65 (2002) 055801.

[6] Y. Parpottas, S. M. Grimes, S. Al-Quraishi, C.R. Brune, T.N. Massey, J.E. Oldendick, A. Salas, T. Wheeler, Phys. Rev. C 70 (2004) 065805.

[7] P.N. Replowski, L.T. Baby, I. Wiedenhöver, S.E. Dekat, E. Diffenderfer, D.L. Gay, O. Grubor-Urosevic, P. Höflich, R.A. Kaye, N. Keeley, A. Rojas, A. Volya, Phys. Rev. C 79 (2009) 032801(R).

[8] D. Seweryniak, P.J. Woods, M.P. Carpenter, T. Davinson, R.V.F. Janssens, D.G. Jenkins, T. Lauritsen, C.J. Lister, J. Shergur, S. Sinha, A. Woehr, Phys. Rev. C 75 (2007) 062801(R).

[9] T. Komatsubara, K. Ebisu, T. Kawamata, A. Ozawa, K. Hara, T. Moriguchi, Y. Hashizume, T. Shizuma, T. Hayakawa, S. Kubono, UTTAC Annual Report 2007, UTTAC-77 (2008) pp. 15-16.

[10] T. Komatsubara, A. Ozawa, K. Hara, T. Moriguchi, Y. Ito, H. Satake, H. Ooishi, Y. Ishibashi, T. Shizuma, T. Hayakawa, S. Kubono, S. Hayakawa, D.N. Binh, A. Chen, J. Chen, UTTAC Annual Report 2008, UTTAC-78 (2009) pp. 13-14

[11] C. Rolfs and W. Trost, Nucl. Phys. A 122 (1968) 633

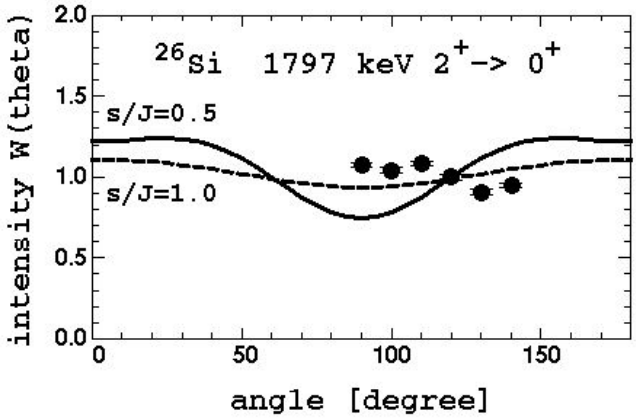

Fig. 1 Angular distribution of 1797 keV gamma ray.

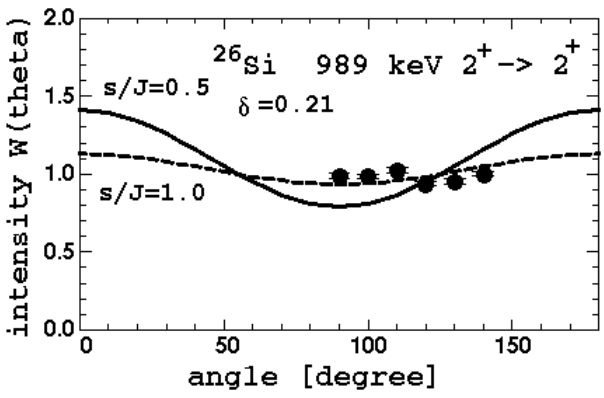

Fig. 2 Angluar distribution of 989 keV gamma ray.

2.3 Confirmation of Star anomaly and QFS anomaly in *pd* breakup

K. Sagara[1], S. Kuroita[1], T. Yabe[1], K. Ishibashi[1], T. Tamura[1], M. Okamoto[1], Y. Maeda[2],
Y. Tagishi, T. Komatsubara, A. Ozawa, Y. Ishibashi, Y. Ito, H. Ooishi, K. Yokoyama, Y. Abe,
S. Fukuoka, S. Nakamura, K. Okumura, S. Ito, R. Nishikiori, T. Niwa, and T. Yuasa

In three nucleon breakup reactions, there is a curious phenomenon of Star anomaly whose origin has not known for over 20 years. When outgoing three nucleons form an equilateral triangle, the configuration is called as Star. We define an angle α between the triangle and the beam axis as shown in Fig. 1. The configuration at $\alpha = 90^{\circ}$ is called as Space Star. At Space Star, measured cross section is about 25% higher than calculation in *nd* breakup at $E_n = 13$ MeV [1,2], and about 15% lower than calculation in *pd* breakup at $E_p = 13$ MeV [3,4].

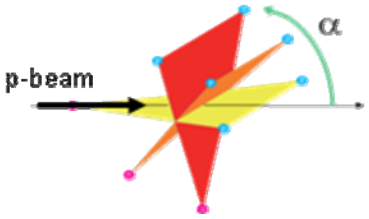

Fig. 1. Definition of the inclination angle α of Star in the c.m. system.

Systematic measurements of α-dependence of Star anomaly have been made by Kyushu group at E/A = 13 MeV and 9.5 MeV, and by Koeln group at E/A = 9.5 MeV (E_d =19 MeV). Kyushu data indicate that Star anomaly appears only around $\alpha = 90^{\circ}$. Koeln group reported enormous Star anomaly of 25% at $\alpha = 124^{\circ}$- 156°[5]. Whether Star anomaly occurs only around $\alpha = 90^{\circ}$ or in a wide α range is a big problem to investigate the origin of Star anomaly.

We therefore made a confirming experiment of Koeln data at the same energy and at the same angular range at UTTAC. A 19 MeV unpolarized *d*-beam was incident on a rotating CD_2 foil target, and two protons from $d+p \rightarrow p+p+n$ reaction were detected in coincidence. Simultaneous measurements at $\alpha = 120^{\circ}$, 140°, 160° and 180° were made using eight Si detectors. Apertures in front of the detectors were made in a fine machinery factory. A monitor detector was used to measure *p*+*d* scattering, and absolute value of *pd* breakup cross section was determined using precise cross section of *pd* scattering measured at Kyushu [6].

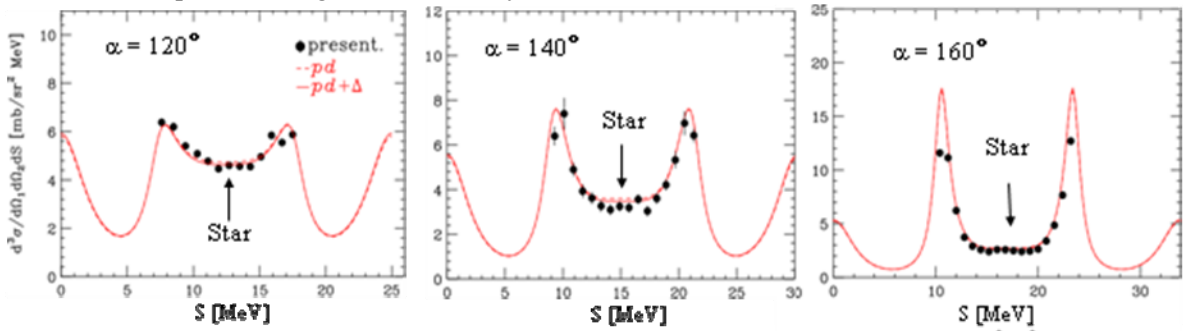

Fig. 2. Measured $H(d,p_1p_2)n$ cross section at $E_d = 19$ MeV. Curves are *pd* calculation by A. Deltuva [7].

[1] Department of Physics, Kyushu University, Hakozaki 6-10-1, Fukuoka 812-8581, Japan
[2] Department of Applied Physics, Miyazaki University, Konohanadai-Nishi 1-1, Miyazaki 889-2192, Japan

Typical results are shown in Fig. 2. The present data at α = 120°- 180°agree with calculation, contrary to Koeln data at α = 124°- 156°which are 25% lower than calculation. Koeln group used a polarized *d*-beam to measure A_y and A_{yy} together with cross section. We used an unpolarized *d*-beam to measure the present cross section. We have measured Star cross section at Kyushu University, RCNP and UTTAC in the same method,

In Fig. 3 α-dependence of Star anomaly at E/A = 9.5 MeV and 13 MeV is shown. Our data including the present ones indicate that Star anomaly occur only around α = 90°at both E/A = 9.5 MeV and 13 MeV, and the α-dependence varies gradually with the incident energy.

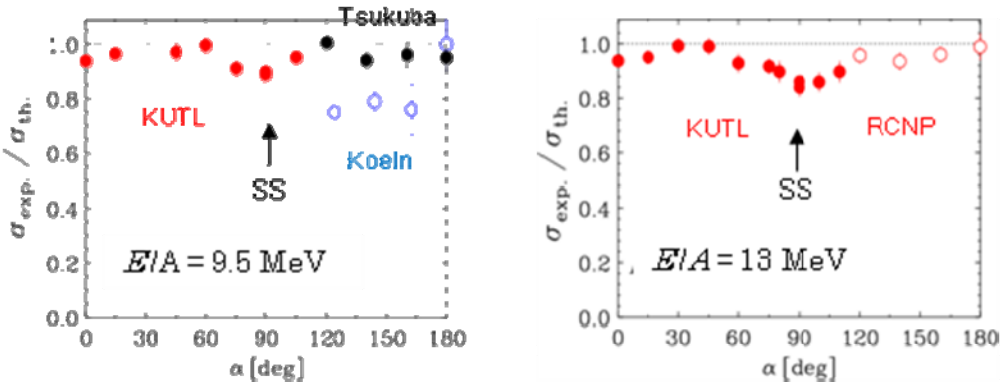

Fig. 3. α-dependence of *pd* Star cross section at E/A = 9.5 MeV and 13 MeV.

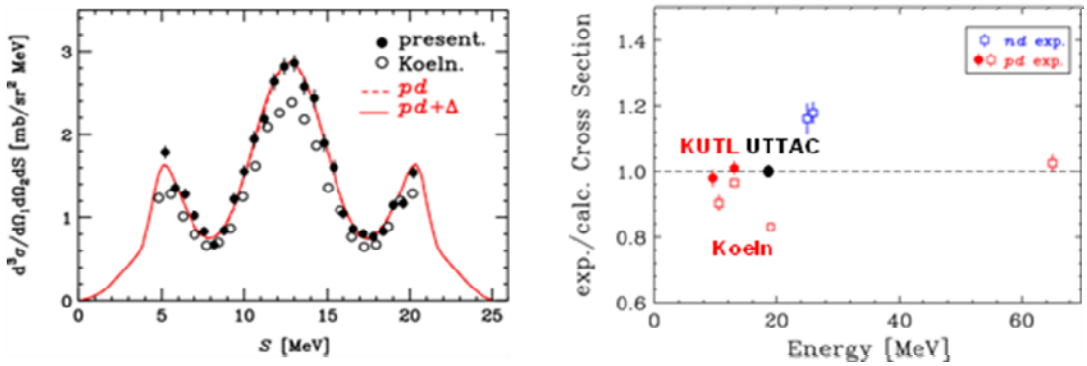

Fig. 4. (Left) Cross section around *pd* QFS at E_p=19 MeV. (Right) Energy dependence of *pd* QFS anomaly.

We also measured cross section of *pd* QFS (Quasi Free Scattering) using at E_p = 19 MeV. An unpolarized 19 MeV *p*-beam was incident on a rotating CH_2 target foil. Measured cross section agrees with *pd* calculation as seen in Fig. 4, contrary again to Koeln data [8]. Energy dependence of QFS anomaly in Fig. 4 suggests that there is no QFS anomaly in *pd* breakup.

References

[1] J. Strate et al., Nucl. Phys. **A501** (1989) 51
[2] H. R. Setze et al., Phys. Lett. **B388** (1996) 229
[3] H. Rauprich et al., Nucl. Phys. **A535** (1991) 313
[4] T. Ishida et al., Mod. Phys. Lett. **A18** (2003) 436
[5] J. Ley et al., Phys. Rev. **C73** (2006) 064001
[6] K. Sagara et al., Phys. Rev. **C50** (1994) 576
[8] H. Patberg et al., Phys. Rev. **C53** (1996) 1497
[7] A. Deltuva et al., Phys. Rev. **C72** (2005) 054004; A. Deltuva, private communication

2.4 Inelastic scattering of 30 MeV alpha particle from ^{12}C

R.Nishikiori, H.Suzuki, A.Ozawa, D.Nagae, T.Moriguchi, Y.Ishibashi, H.Ooishi, K.Yokoyama, Y.Abe, K.Okumura, S.Fukuoka, S.Ito, T.Niwa, S.Kubono[1], and A.A.Ogloblin[2]

Hoyle state, which is an excited state of ^{12}C, was predicted with cosmic nucleosynthesis. This state has 3 α-cluster structures. It deeply deals with the production of ^{12}C from 3 αs in stars. The energy of Hoyle state is 7.65 MeV, and its spin-parity is 0^+ [1]. It is considered that the cluster structure makes the radius of Hoyle state larger than that of the ground state. In our study, the difference between the radii of Hoyle and the ground state was deduced from diffraction radii of them with α scatterings.

At small scattering angles, the differential cross sections of direct reactions at high energies (>10 MeV/u) obey Frauenhofer diffraction. This diffraction depends on the radii of the targets. Measuring the angular distributions of elastic and inelastic scattering of ^{12}C may be a good method to determine the radius of Hoyle state and the ground state.

Before the experiment, we improved the single wire position sensitive proportional counter (SWPC), which is installed in the spectrometer of E-course. The schematic view of SWPC is shown in Fig. 1. The hit position of charged particles is deduced from charges at both ends of the wire which have resistance of about 6 kΩ/m. To improve the detection length and sensitivity, we changed the followings:

- The length of the wire was changed from 300 mm to 450 mm to enable to measure Hoyle state and the ground state at one measurement.
- Thickness of the wire was changed from 10 μm to 17 μm to stretch tightly.
- New insulation resistances were made to enable the counter to held against high voltage up to 1.9 kV.

The experiment was performed at E-course of UTTAC by using EPS90 spectrograph. The experimental setups are shown in Fig. 2. The beam was 30-MeV α particles, and its intensity was 5 nA. The thickness of the ^{12}C target was 100 μm/cm^2. The counter gas was Ar (70%)+CH_4 (30%). The high voltage of 1.6 kV was applied to the counter. In this condition, Hoyle state and the ground state are easily separated.

The results of the differential cross sections are shown in Fig. 3. Diffraction radii $R_{\rm dif}$ of the light heavy ions are obtained from minima and maxima of angular distribution of differential cross sections of elastic and inelastic scatterings. Although $R_{\rm dif}$ is not the root-mean-square (rms) radius itself, the difference between $R_{\rm dif}$ of two states are the same as that of rms radii [2].

The diffraction radii of the first two minima and maxima of each state are summarized in Table 1. From this experiment, we obtained diffraction radius of the ground state as 5.6$\pm$0.3 fm, and that of Hoyle state as 4.8$\pm$0.3 fm. The rms radius of Hoyle state has been measured to be smaller than that of the ground state of ^{12}C by 0.8$\pm$0.4 fm, which is not consistent with a simple speculation. Possible reason of the result is due to the low primary beam energy. For ^{12}C, at least 10 MeV/A should be needed. Measurement at higher beam energy is required for future experiments.

[1]CNS, Tokyo University
[2]Kurchatov Institute

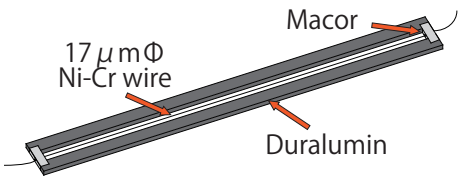

Fig. 1. Schematic view of SWPC.

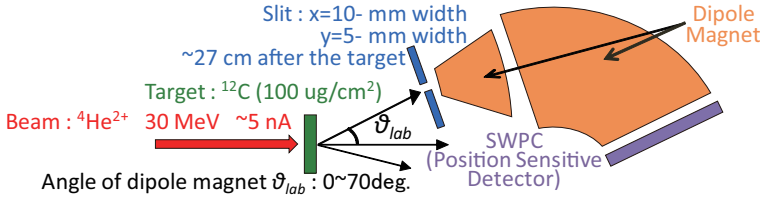

Fig. 2. Experimental setup.

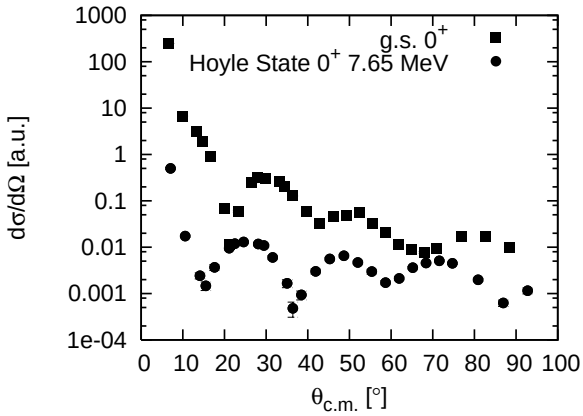

Fig. 3. Differential cross section of scattering of α particles from ^{12}C at 30 MeV. $\theta_{c.m.}$ is the scattering angle in the center of mass system.

Table 1. diffraction radii obtained from $\theta_{\mathrm{c.m.}}$

	$\theta_{\mathrm{c.m.}}[^\circ]$	R_{dif}[fm]	$\langle R_{\mathrm{dif}}\rangle$[fm]
g.s.	21.3±1.0	5.8±0.3	5.6±0.3
	27.9±1.1	6.1±0.2	
	42.9±1.6	5.3±0.2	
	52.4±1.6	5.3±0.2	
Hoyle	15.5±1.1	4.4±0.3	4.8±0.3
	24.6±1.7	4.9±0.3	
	36.4±1.0	5.1±0.1	
	48.7±1.7	5.1±0.2	

References

[1] Richard B. Firestone, Table of Isotopes Eighth Edition Vol.1, (1996)

[2] A. N. Danilov, T. L. Belyaeva, A. S. Demyanova, S. A. Goncharov, A. A. Ogloblin, Phys. Rev. Lett., **C80**, 054603 (2009)

2.5 Production of nuclear polarization for unstable nuclei via polarization transfer reaction

Y. Ishibashi, A. Ozawa, D. Nagae, Y. Abe, S. Ito, H. Suzuki, T. Moriguchi, H. Ooishi, K. Yokoyama, K. Okumura, S. Nakamura, S. Fukuoka, R. Nishikiori, T. Niwa, Y. Tagishi, T. Nagatomo[1] and K. Matsuta[2]

The nuclear moment is one of the most important observables of the nuclear structure. For example, the nuclear magnetic dipole moment (μ) provides us with information on the configuration mixing in the shell structure. For the measurements of the μ of unstable nuclei, β-ray-detected nuclear magnetic resonance method (β-NMR) is effective. In the β-NMR method, unstable nuclei must be spin-polarized. In this work, the nuclear polarization (P) for ^{20}F, ^{41}Sc, ^{24m}Al, ^{29}P and ^{40}Sc isotopes, which were produced by the nuclear polarization transfer reactions, were measured. First, since P of ^{20}F has been measured at UTTAC [1] previously, we measured P of ^{20}F as system check of our system. Second, since μ of ^{41}Sc has been measured using a CaO stopper [2], the measurement of P of ^{41}Sc was performed, to check whether the polarization can maintain inside the CaO pellet produced from CaO powder. Third, spin polarized ^{24m}Al has been produced by using polarized proton beam, to check whether spin polarized isotope can produce by polarized proton beam. Fourth, the μ of ^{29}P has been measured using polarized deuteron beam [3]. We measured P of ^{29}P using polarized proton beam to compare P by the different incident beams.

The experiment was performed at F-course of the first experimental room in UTTAC. The polarized proton/deuteron beams were produced by a Lamb-shift type polarized ion source, and accelerated by a 12UD pelletron accelerator. The polarized beams were transported to the beam line of the F-course and were irradiated to the targets (stopper) to produce the spin polarized radioactive nucleus. The detectors located up and down of the stopper counted the number of β-rays emitted from the produced nucleus. From the obtained NMR effects, the degrees of nuclear polarization were deduced.

Table 1. The degree of polarization for 5 isotopes which magnetic moment of already known.

	^{19}F(d,p)^{20}F	^{40}Ca(d,n)^{41}Sc	^{24}Mg(p,n)^{24m}Al	^{28}Si(d,n)^{29}P	^{29}Si(p,n)^{29}P
E_{Beam}[MeV]	7.0	7.0	20.0	4.0	10.0
AP_{exp} [%]	**-0.60±0.06**	**0.40±0.05**	**0.08±0.04**	**0.35±0.16**	**0.12±0.02**
A	-0.333	0.222	0.088±0.001	0.65	
ε_{Ω} [%]	82^{+8}_{-6}				
ε_{purity} [%]	99.6 ±0.5	86.2 ±1.2	61.3 ±1.9	93.6 ±2.0	51.7 ±0.4
ε_{beam} [%]	76±2	75±1	77±6	67±1	88±1
$P_{present}$ [%]	2.9 ±0.4	3.4 ±0.6	2 ±1	1.1 ±0.5	0.49 ±0.10
$P_{reference}$ [%]	~3 [1]	~3.8 [2]			

[1] International Christian University
[2] Osaka University

Table 1 shows experimental results of degree of nuclear polarization (AP_{exp}) for 5 isotopes in which magnetic moments are already known. Here, the experimental AP_{exp} can be corrected to deduce the real polarization degree. We corrected by 1) asymmetry parameter of β-rays (A), 2) polarization degree of the incident beam (ε_{beam}), 3) purity of β-rays (ε_{purity}), and 4) finite solid angle of detectors (ε_{Ω}). The results of corrected degree of polarization are shown by $P_{present}$ in Table 1.

From comparison of the obtained $P_{present}$ and $P_{reference}$ for ^{20}F, we found that our system worked property. And from comparison of the obtained $P_{present}$ and $P_{reference}$ for ^{41}Sc, we confirmed polarization of ^{41}Sc maintained inside present CaO pellet. Moreover, from $P_{present}$ of ^{24m}Al and ^{29}P, we confirmed to produce spin polarized nucleus via polarization transfer reaction using proton beam. From the results of ^{29}P, the measured polarization $P_{present}$ using the polarized deuteron beam was found to be larger than that using the polarized proton beam.

In the present measurements, we also searched μ for ^{40}Sc. Fig.1 shows measured NMR spectrum of ^{40}Sc. Red (Blue) points are data measured by static magnetic field H_0 = 0.37 T (0.30 T) respectively. From the results, μ of ^{40}Sc has not been clearly determined. We will continue the measurements in future experiments.

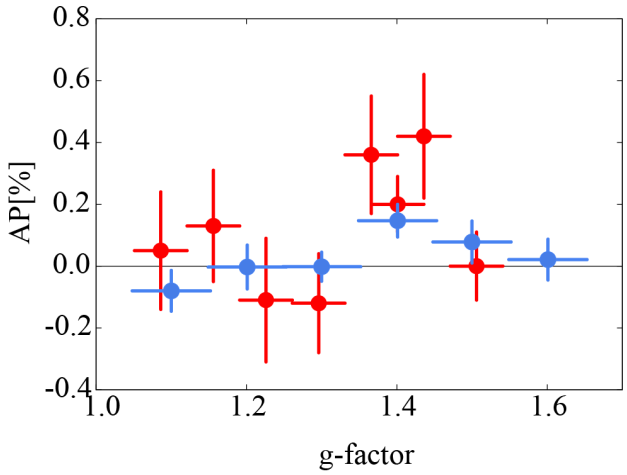

Fig.1 NMR spectrum of ^{40}Sc

References

[1] K. Matsuta et al., UTTAC ANNUAL REPORT 2004(2005)14

[2] T. Minamisono et al., Nucl. Phys. A516(1990)365

[3] Y. Abe et al., UTTAC ANNUAL REPORT 2009(2010)13

2.6 Development of the time-of-flight detector for rare-RI ring in RIKEN RIBF

Y. Abe, D. Nagae, A. Ozawa, T. Moriguchi, H. Suzuki, Y. Ishibashi, S. Ito, Y. Ito, H. Ooishi, K. Okumura, S. Fukuoka, S. Nakamura, R. Nishikiori, T. Niwa, K. Yokoyama

A construction of the isochronous storage ring for precision mass measurements of rare-RI has been planned at RIKEN RI Beam Factory (RIBF) [1]. In this plan, RIs produced by projectile fragmentation and/or uranium fission, which will be identified by using the BigRIPS fragment separator [2], will be injected into the storage ring (rare-RI ring) individually. The revolution times of the RIs will be measured by using a time-of-flight method (TOF) to evaluate. masses of the RIs. Details for the principle of the mass measurement are described elsewhere [3].

In order to determine the value of mass with a precision of 10^{-6}, requirements for the TOF detector in rare-RI ring are follows; i) good time resolution less than 100 ps, ii) small energy loss, iii) unchanging of the charge state by passing through a detector, iv) a large acceptance aperture because of the large beam size in the rare-RI ring. In order to satisfy these requirements, a TOF detector using a micro channel plate (MCP) has been developed (named by MCP-TOF). Time pick-off system of our MCP-TOF is following. A beam generates secondary electrons in passing through a thin carbon foil. These electrons are transported to a MCP by electric and magnetic fields. A schematic view of the MCP-TOF is shown in Fig. 1. The size and thickness of carbon foil is 100 × 50 mm^2 and 60 μg/cm^2. In order to create a uniformed electric field, eleven electrodes installed in the MCP-TOF are connected using 2.2 MΩ resisters at 6.0 mm intervals. To make a magnetic field, two coils (100 turn) are placed both side of the MCP-TOF. To achieve an isochronous condition, an electric (E) and a magnetic (B) fields, and a horizontal displacement of the secondary electrons (D) are satisfied a relation [4]

$$D = \frac{2\pi m}{q}\frac{E}{B^2},$$

where m and q denotes a mass and a charge of electron, respectively. In the case of the present MCP-TOF, the horizontal displacement is chosen as D = 140 mm, thus the electric and the magnetic field are calculated to be E = 17143 V/m and B = 20.9 G.

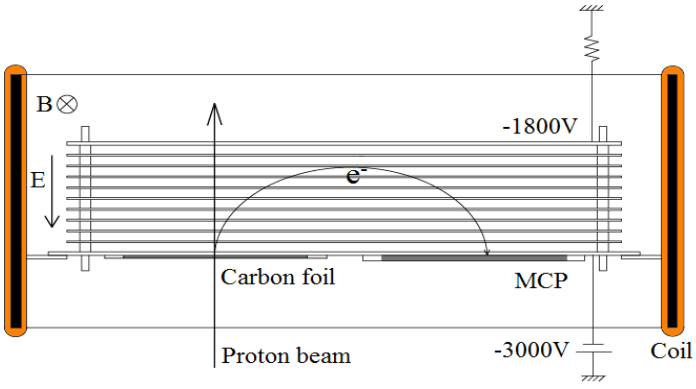

Fig.1. Schematic view of our MCP-TOF

An experiment to evaluate a time resolution of the MCP-TOF (σ_t) was performed at the F-course beam line in UTTAC. The experimental setup is shown in Fig. 2. Proton beam (18 MeV) was transported to the MCP-TOF located downstream of the Q-D-Q magnets. To generate a start signal of TOF, a plastic scintillator was located just upstream of the MCP-TOF which produced a stop signal of TOF. The beam rate at the plastic scintillator was adjusted about 2.0 × 10^3 cps by scattering with a gold foil located at the scattering chamber. We measured a TOF between the plastic scntillator and the MCP detector. In this experiment, E and B set to about E = 17143 V/m and B = 19.4 G. A typical TOF spectrum is shown in Fig. 3. The time resolution is obtained to be σ_t = 0.91 ± 0.01 ns by fitting the TOF spectra with a Gaussian function. The obtained time resolution is included time dispersion component due to an energy straggling of proton beam. To determine an intrinsic time resolution of the MCP-TOF, an estimation of the time dispersion is in progress with SRIM code [5].

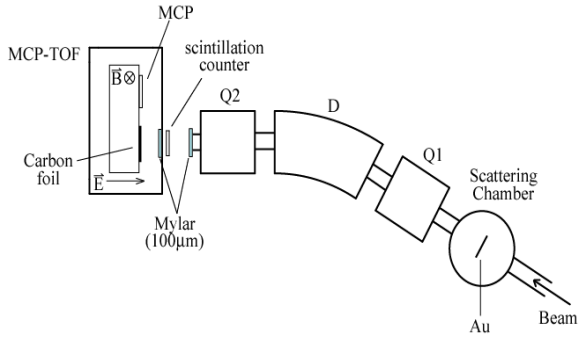

Fig.2. Schematic view of F-course beam line

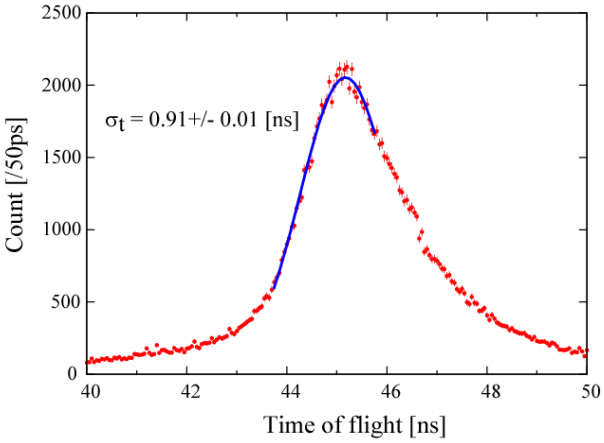

Fig.3. TOF spectrum with a Gaussian fitting

In summary, the time resolution of MCP-TOF is deduced to be σ_t = 0.91 ± 0.01 ns by using a 18 MeV proton beam. To obtained good time resolution less than 100 ps, we are going to simulate this system with GEANT4 [6].

References

[1] Y. Yano, Nucl. Instr. and Meth. B 261 (2007) 1009.

[2] T. Kubo, Nucl. Instr. and Meth. B 204 (2003) 97.

[3] Y. Yamaguchi, et al., Nucl. Instr. and Meth. B 266 (2008) 4575.

[4] J. D. Bowman, R. H. Heffner, Nucl. Instr. and Meth. 148 (1978) 503.

[5] J. F. Ziegler, Nucl. Instr. And Meth. B 219-220 (2004) 1027.

[6] S. Agostinelli, et al., Nucl. Instr. and Meth. A 506 (2003) 250.

2.7 Search of neutron halo in ^{9}Be excited states

A.S. Demyanova[1], A.N.Danilov[1], S.V.Dmitriev[1], A.A.Ogloblin[1], S.A.Goncharov2, N.Burtebaev[3], J.Burtebaeva[3], N.Saduev[3], T.L.Belyaeva[4], H.Suzuki[5], R.Nishikiori[5], A.Ozawa[5], D.Nagae[5], T.Moriguchi[5], Y.Ishibashi[5], H.Ooishi[5], K.Yokoyama[5], Y.Abe[5], K.Okumura[5], S.Fukuoka[5], S.Ito[5], T.Niwa[5], T.Komatsubara[5], S.Kubono[6]

[1] *Kurchatov Institute, Moscow, Russia*

[2] *Scobeltzin Institute of Moscow State University, Moscow, Russia*

[3] *Institute of NuclearPhysics, Almati, Kazakhstan*

[4] *Mexico University, Mexico, Mexico*

[5] *Institute of Physics, University of Tsukuba, Japan*

[6] *Center of Nuclear Science, University of Tokyo, Japan*

It was shown in Ref. [1] that the first excited state $1/2^{+}$, 1.68 MeV of ^{9}Be located at ~ 15 keV above a neutron emission threshold and occupying the s-state might have abnormally large radius typical to neutron halos. This conclusion was drawn from the analysis of the ^{9}Be + α inelastic diffraction scattering at 35.5 MeV [2]. In order to get independent confirmation of this result and to look for the effect in the other excited states of ^{9}Be we studied ^{9}Be + α scattering at University of Tsukuba tandem accelerator at $E(\alpha)$ = 30 MeV. The diffraction radii R_{dif} of the ^{9}Be states were extracted from the measured positions of the minima and maxima of the relevant angular distributions. The "real" (say, *rms*) radii R^* of the ^{9}Be excited states can be obtained [3] from the relation

$$R^* = R_0 + [R_{dif}^* - R_{dif}(0)],$$

where R_0 denotes the *rms* radius of the ground state.

Energy spectra were measured by the Enge type magnetic spectrograph. The interval of the ^{9}Be excitation energies reached ~ 12 MeV. The angular distributions were measured up to ~ 140°. The analysis of all the data is not yet completed, and this report contains preliminary results some of which could be changed in future.

A typical spectrum is shown in Fig.1. ^{9}Be has developed α + α + n cluster structure. Two rotational bands are known: $3/2^{-}$(0.00) – $5/2^{-}$(2.43) –

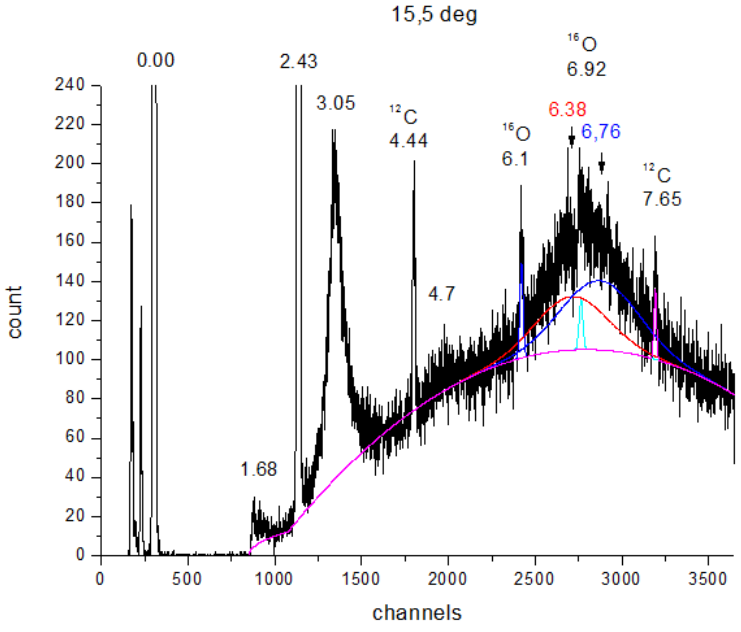

Fig.1. Energy spectrum at 15.5°. Red and blue lines above the background denote the results of the decomposition of the bump at ~ 6.5 MeV into two groups corresponding to the states at E* = 6.38 and 6.76 MeV

$7/2^-(6.38)$ and $1/2^+(1.68) - 5/2^+(3.05) - 3/2^+(4.70) - 9/2^+(6.76)$. All these states are seen. Both highest members of the π- and σ- bands form the broad unresolved bump at ~6.5 MeV. The background was calculated as the sum of two 3-body phase volumes near the ^{8}Be + n and ^{5}He + ^{4}He thresholds and extrapolated by a polynomial of the 2nd order to the higher excitation energy region.

The differential cross-sections of the elastic and inelastic (with the excitation of 1.68 MeV state) are shown in Fig.2. The transition to the $1/2^+$ state is characterized by a single angular momentum transfer L = 1, and the positions of the angular distribution extremes should be in phase with those of the elastic scattering. A clear shift of the inelastic data to the forward angles is seen, and this is an indication of the inelastic diffraction radius enhancement. The extracted values of the diffraction radii are presented in Table1.

Table 1. Diffraction radii of ^{9}Be states (preliminary results)

E, MeV, I^π	R_{dif},fm	$R_{dif}(E^*) - R_{dif}(0.00)$ This work	R_{dif}, fm	$R_{dif}(E^*) - R_{dif}(0.00)$ Ref.[1]
0.00, $3/2^-$	5.71±0.04	-	5.49±0.06	-
1.68, $½^+$	7,55±0.16	1.84±0.17	6.64±0.14	1.15±0.16
2.43, $5/2^-$	5.55±0.05	- 0.16±0.06	5.53±0.05	0.04±0.07
3.05, $5/2^+$(L=1)	6.70±0.60	0.99±0.60	> 6.6	> 1.1±0.6
3.05, $5/2^+$(L=3)	6.24±0.38	0.53±0.39		

The main result is that the 1.68 MeV state really has the enhanced diffraction (and correspondingly, rms) radius in accordance with conclusion of Ref. [1]. Formation of the other excited states admits more than one L-value, and extraction of the diffraction radii requires a more elaborate analysis. This will be done in the course of the coupled channel calculations.

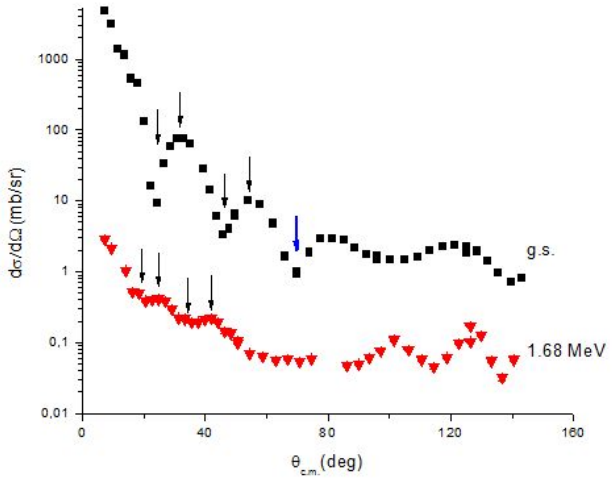

Fig.2 Differential cross sections of ^{9}Be+α and inelastic (to 1.68 MeV, $1/2^+$ state). Arrows denote the positions of extremes used for determining diffraction radii.

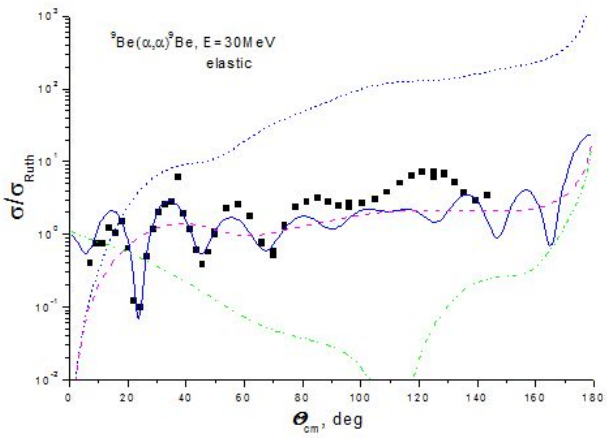

Fig.3. Differential cross sections of ^{9}Be+α elastic scattering. Dashed and dotted (W=0) curves denote the far component.

Decomposition of the elastic scattering cross-section into far and near components shows that the minimum at about 70^o (Fig.3) probably is connected with the nuclear rainbow phenomenon. According to [1], the enhanced radius of the 1.68 MeV state should lead to the shift of the corresponding minimum in the inelastic differential cross-section to the larger angles by 20 – 25 degrees which would provide an independent tool of measuring the radius. However, strong backward oscillations clearly observed [4] in the elastic and inelastic (to the 2.43 MeV state) scattering appear in this angular range and do not allow making definite identification of the rainbow pattern without coupled channel calculations. Study of these oscillations has self-dependent importance because it would reveal the ^{5}He transfer process to ^{4}He and allow estimating of corresponding spectroscopic factors in different states including $1/2^+$ one.

References

[1] A.A.Ogloblin et al., AIP Conf. Proc. 1224 (2010) 100; Int. J. Modern Phys. E 20 (2011) N 5 (to be published).

[2] R.J.Peterson, Nucl. Phys. A 377 (1982) 41

[3] A.N.Danilov et al., Phys. Rev. C 80, (2009) 054603

[4] N.Burtebaev et al., Journal of Nuclear Physics, 55 (1992) 577 and to be published.

3.

MATERIALS AND CLUSTER SCIENCE

3.1 Mössbauer study on the antiferromagnetic FeO synthesized under high pressure

T. Yoshikawa, Y. Kanke,[a] H. Yanagihara, and E. Kita
[a]National Institute of Materials Science, Tsukuba

A series of 3d metal mono oxides, MO (M= Mn, Fe Co and Ni), have a simple NaCl crystalline structure and their electronic states have been investigated intensively. The simple crystalline environments produce a typical energy change in their electronic systems according to the crystalline field. In the case of MnO and NiO, magnetic moments lie in (111) plains due to the quench of orbital moments, however the orbital angular momenta remain in FeO and CoO, where electron orbits are degenerated in $d\varepsilon$ orbits. In the case of CoO, the direction of magnetic moments deviated from (100) due to the orbital moments. For FeO, the difficulty in the sample preparation has been pointed out. The Fe defects are commonly detected in samples and the amount of the iron, x, has not exceed 0.96 in the Fe_xO formula. It makes understanding of the essential properties difficult. It was reported that the stoichiometric FeO can be obtained by the sample preparation under the high pressure.[1] In this study, we performed Mössbauer study on the samples prepared with the high pressure synthesis technique in order to evaluate the Fe defects with different conditions of the preparation.

Samples were synthesized using a modified belt-type high pressure and high temperature apparatus installed in NIMS.[2] The starting materials were prepared by mixing α-Fe and Fe_2O_3 powder in an atomic ratio of Fe:O = 1:1 and were heated up to T_S = 1000 ∼ 1200 °C under 5.5 GPa for 1 hour.

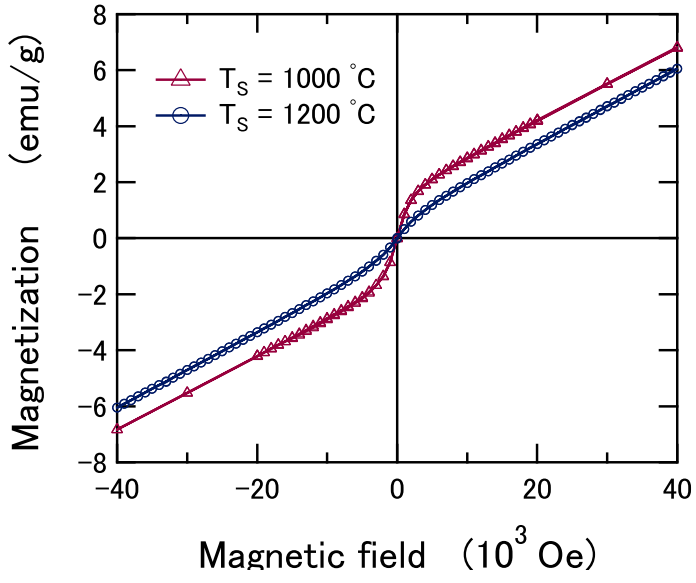

Fig. 1. Magnetization curves for FeO prepared under high pressure and high temperature.

The synthesized samples were examined with powder X-ray diffraction. The samples were revealed to be in an NaCl type single phase and no trace of other compounds were detected. Magnetization measurements were carried out with a conventional SQUID magnetometer. The magnetization curves recorded

at room temperature were shown in Fig. 1. Small amount of ferromagnetic components is clearly seen in both magnetization curves. Assuming that residual ferromagnetic parts are composed of α-Fe, the amounts are estimated to be 0.69 at% for the T_S = 1000 °C sample and 0.24 at% for the T_S =1200 °C sample, respectively. From this result, higher reaction temperature may bring lower concentration of ferromagnetic components.

Mössbauer study was carried out at room temperature. The obtained spectra are shown in Fig. 2. Since the Néel temperature of FeO is around 200 K, much lower than room temperature, paramagnetic spectra were observed.

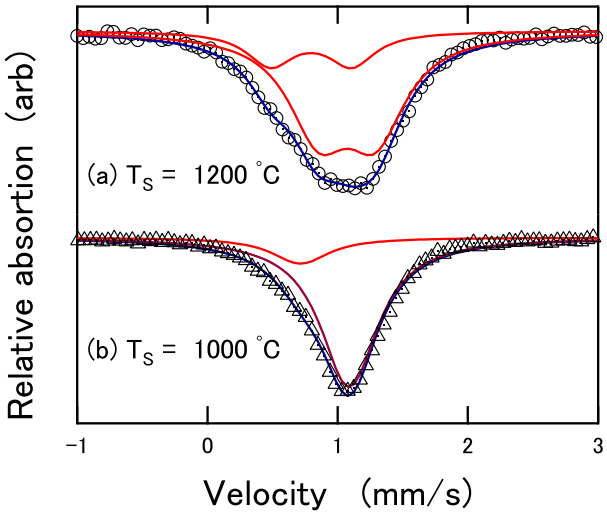

Fig. 2. Mössbauer spectra recorded at room temperature for FeO samples prepared under high pressure and high temperature. The reaction temperatures were (a) T_S =1200 °C and (b) T_S =1000 °C, respectively.

The relatively sharp line width of the spectra was observed for the T_S = 1000 °C sample and the line shape can fit to the combination of a major singlet and an additional minor singlet.(Fig.2(b)) This implies that the environment for Fe ions is almost identical. However, at least the two kinds of Fe sites with lower symmetry exist in the T_S =1200 °C sample. From these results, it is resulted that more uniform sample in terms of the Fe local environment is established in lower T_S samples, but the amount of residual ferromagnets has pointed to an opposite trend.

We would like to thank Prof. Siratori for valuable discussion and encouragement.

References

[1] T. Katsura, B. Iwasaki, and S. Kimura, J. Chem. Phys. **47** (1967) 4559.

[2] T. Taniguchi, M. Akaishi, Y. Kanke, S. Yamaoka, Rev. Sci. Inst. **75** (2004) 1959-1962.

3.2 Study on the diffusion of nitrogen atoms in Fe submicron particles using Mössbauer spectroscopy

M. Minagawa, H. Yanagihara, M. Kishimoto and E. Kita

Iron nitrides[1][2] are categorized as interstitial compounds, and changes their magnetic properties and crystal structures with the composition ratio of iron and nitride. They are composed of ubiquitous elements, so have high potentials as environmentally-enhancing materials being alternatives of current permanent magnets and spin-polarized materials. α"-$Fe_{16}N_2$ has high uniaxial magnetic anisotropy and large saturation magnetization, so it can be applied for high performance permanent magnet or magnetic recording media. γ'-Fe_4N has been predicted as a half-metallic material, then it can be used for spintronics devices. ε-$Fe_{2-3}N$ is the most stable compound and has uniaxial magnetic anisotropy be attributed to its hcp structure.

These ferromagnetic iron nitrides have been focused because of its magnetic properties. It is important to clarify the nitrogen diffusion process more quantitatively because the characteristics are affected by the production process in such interstitial compounds. Many studies have been done on bulk two-dimensional model[3], but knowledge in particle is a few. This arises from the surface coat of each particle and particle becomes two-phase, its diffusion model becomes more complicated. Additionaly Mössbauer spectroscopy is suitable to observe nano-sized structures including ^{57}Fe atoms.

In this report, we fabricated submicron-size nitride particle with the maximum diameter that can be obtained stable single-phase α"-$Fe_{16}N_2$[4]. Using Mössbauer spectroscopy, iron-nitride samples with various reaction conditions were analyzed from the view point of nitrogen diffusion.

Commercially available 130-nm and 180-nm Fe_3O_4 particles (Toda Kogyo Corp.) were used as starting materials and were reduced in an H_2 gas flow at 673 K for 2.5 h. The reduced samples were then successively nitrided in an NH_3 gas flow for 24 h at various temperatures. X-ray diffraction (XRD) study was carried out for identification of resulted phase. Samples for Mössbauer spectroscopy were sealed in epoxy resin to prevent the oxidation. Mössbauer spectra were recorded at room temperature and data were numerically analyzed with a commercially available fitting software, MossWinn ver.3.

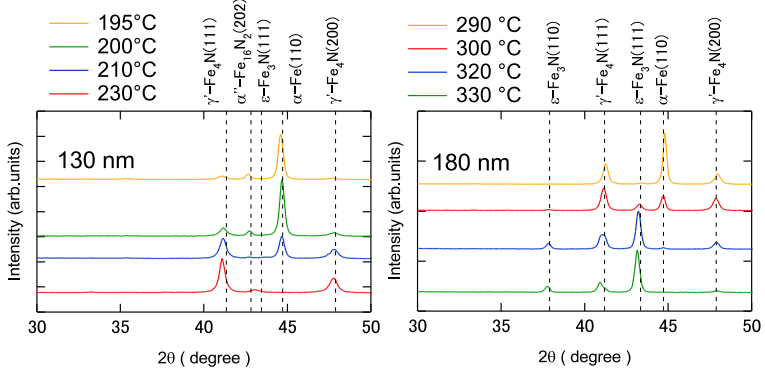

Fig. 1. XRD patterns of 130-nm(left) and 180-nm(right) iron nitride particles.

The samples reduced from the Fe_3O_4 particles were confirmed to be in an α-Fe single phase for

both diameters (not shown). The XRD patterns of the samples are shown in Fig.1. Samples with 130-nm diameter were fully nitrided at 230 °C and their nitrided phases were mainly took over γ'-Fe_4N. In contrast samples with 180-nm diameter were fully nitrided at 330 °C and were mainly composed of ε-$Fe_{2-3}N$. These results shows that the difference of 50-nm diameter comes down to the differences of the nitrided temperature about 100 K and their nitrided phases.

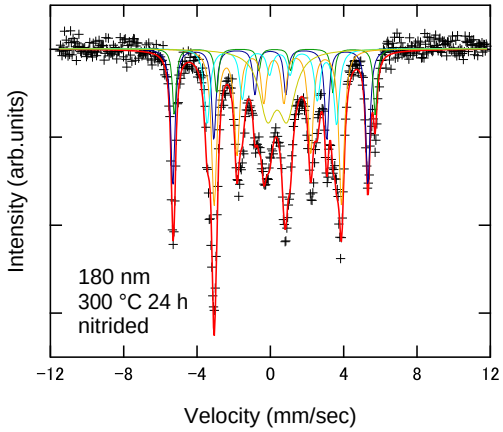

Fig. 2. Mössbauer spectrum for 180-nm particle nitrided at 300 °C for 24 h in NH_3 flow.

To understand this phenomenon, the thermal diffusion process of nitrogen atoms was investigated quantitatively using Mössbauer spectroscopy. Figure 2 shows an example of Mössbauer spectra of iron-nitride particles. From the Mössbauer spectra, we can obtain the ratio of the each phase, and then estimated the volume ratio using their crystalline structures. We assume that the samples are spherical particles with α-Fe core and iron nitride shell, and the volume ratio turns into the nitrided depth, χ. This quantity is a function of temperatures, and then the activation energy for the formation of nitrided phase, Q^N_{eff}, was derived for the sample with each diameter. The diffusion in sphere-shaped samples can be written as a one-dimensional system[5] in the same way to bulk-like samples,

$$\frac{\partial u}{\partial t} = D\frac{\partial^2 u}{\partial r^2}, \tag{1}$$

where u is defined to be $u = cr$ and c, D and r are the concentration, the diffusion constant and the radial distance, respectively. Using the nitridation depth (χ), the average mol volume of γ' and ε phases (Ω), and the concentration difference across the phase boundary (Δc), Eq. 1 can be changed to the following formula[6] ;

$$\ln\,\chi = \frac{1}{2}\,\ln(2\,\Omega\,\Delta c\,D_0) + \frac{1}{2}\ln\,\tau - \frac{Q^N_{eff}}{2RT}. \tag{2}$$

Here, τ and R are the nitridation duration and the gas constant, respectively. We also assumed that the effective coefficient D^N_{eff} was separated into the non-temperature-dependent diffusion coefficient D_0 and the activation energy Q^N_{eff}. The Eq. 2 implies that Q^N_{eff} can be obtained from the gradient in the Arrhenius plot.

Prior to the present work, studies on coarse-grained foils[7] and nanocrystalline foils[6] were reported. Figure 3 shows the Arrhenius plots of nitridation depth versus the inverse of nitridation temperature. The

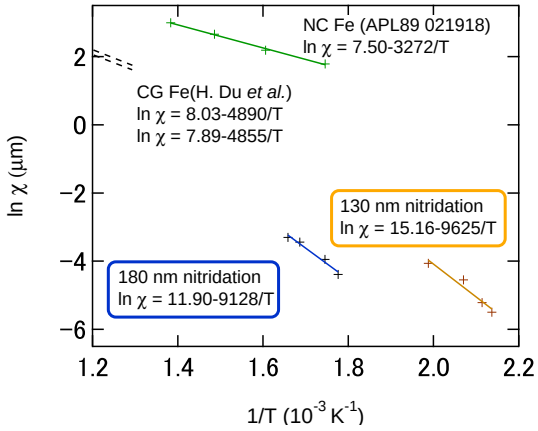

Fig. 3. Temperature dependence of the nitridation depths. Our experimental results of submicron particles are shown in below of figure and results of bulk[6][7] from previous works locate above.

activation energies Q^N_{eff} are 162.7 kJ/mol in 130-nm particles and 169.0 kJ/mol in 180-nm respectively, that are nearly the same amplitude and about twice of the coarse-grained bulk value[7] (Q_ε=80.7 kJ/mol and Q_γ'=88.3 kJ/mol) and three times larger than nanocrystalline bulk one[6] (Q^N_{eff}=54.39 kJ/mol). The difference of the diffusion mechanisms between particles (present work) and bulk foils is clearly seen. This difference may be due to the anti-sintering surface coat of particles disturbing the diffusion of nitrogen atoms. It was reported that the diffusion of nitrogen atoms through a Ni/Fe_3C/Fe structure was disturbed by the Fe_3C layer, and diffusion constant of whole system decrease about three order[8].

According to this phenomenon, the nitrogen concentration in the outer shell of particles was much low, the supply of nitrogen atoms for an iron core was not sufficient to grow the iron nitride phase equal to non-coated samples. As a result, the nitridation depth χ was restricted and the activation energy Q^N_{eff} became higher.

References

[1] J. M. D. Coey, P. A. I. Smith, J. Magn. Magn. Mater. **200** (1999) 405.

[2] M. Takahashi, H. Shoji, J. Magn. Magn. Mater. **208** (2000) 145.

[3] T. Liapina, A. Leineweber, E. J. Mittemeijer, Met. Mat. Trans. **37A** (2006) 319.

[4] S. Kikkawa, A. Yamada, Y. Masubuchi, T. Takeda, Mat. Res. Bull. **43** (2008) 3352.

[5] T. Heumann, *Diffusion in Metallen* (Springer-Verlag, Berlin, 1992).

[6] W. P. Tong, *et al.*, Appl. Phys. Lett. **89** (2006) 021918.

[7] H. Du and J. Ågren, Z. Metallkd. **86** (1995) 522.

[8] M. Nikolussi, A. Leineweber, E. J. Mittemeijer, Phil. Mag. **90** (2010) 1105.

3.3 Hydrogen mapping in Pd-Mg-Ti multi-layer by ambient NRA

D. Sekiba, S. Harada and K. Fukutani[1]

Mg-based nano-scale multi-layer devices have attracted much attention from the viewpoint of the hydrogen storage for the fuel-cell vehicle. Mg absorbs much hydrogen (7.6 wt. %), though it requires too high temperature for the hydrogen desorption in a realistic condition. The nano-scale lattice contraction at interfaces between Mg and other metals is expected to decrease the hydrogen desorption temperature.

We prepared a multi-layer device consisting of Pd (20 nm)/Mg (20 nm)/Ti (10 nm)/Mg (20 nm)/Ti (10 nm)/Si substrate. Previously Baldi *et al.*, reported that the Mg layer near the substrate is selectively hydrogenated at a low pressure of the hydrogen atmosphere < 10^2 Pa due to the constraint at the interface. However, this selective hydrogenation is deduced indirectly by means of the optical reflection measurements. We tried to observe this novel hydrogenation process directly by the newly developed ambient NRA (Nuclear Reaction Analysis).

The beam-line for the ambient NRA has been developed in MALT in University of Tokyo. The 6.4 MeV ^{15}N ion is extracted beyond a thin SiN membrane (100 nm thick and 5 nm Au coated). The reaction of ^{1}H(^{15}N, αγ)^{12}C was used for the hydrogen depth profile. The hydrogen pressure in the cell, in which the multi-layer sample was put, can be changed gradually from 10^{-3} ~ 10^5 Pa by using a combination of turbo pump and a variable leak valve. The distance between the SiN membrane and the sample surface was set at 0.1 mm.

The figure shows the obtained γ-ray yield profile dependent on the ^{15}N beam energy at various pressure hydrogen atmosphere 10^1 ~ 5x10^2 Pa. We can see that the γ-ray signal from the gas phase hydrogen is negligibly small compare to that from the multi-layer sample. By increasing the pressure of hydrogen gas, we can clearly see that the Mg layer near the substrate is selectively hydrogenated, while the Mg layer near the surface is remained little hydrogenated. We are planning to make measurements with higher pressure of the hydrogen atmosphere.

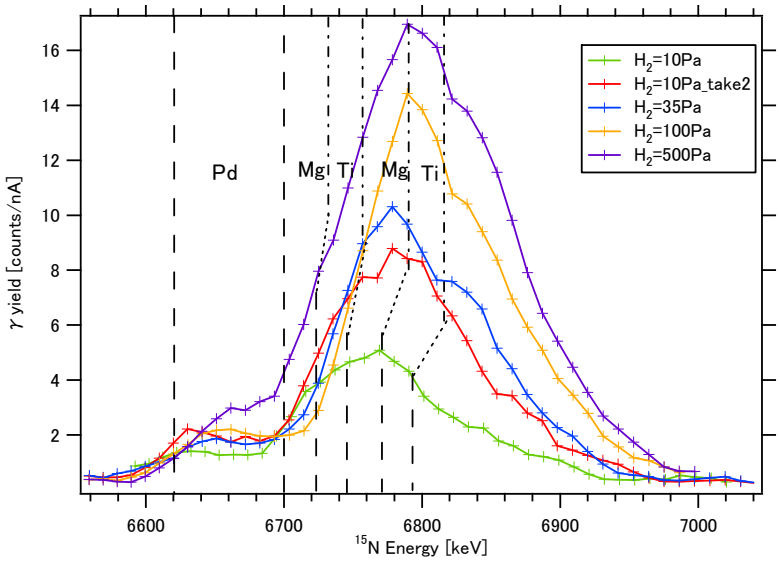

References

[1] A. Baldi, M. Gonzalez-Silveira, V. Palmisano, B. Dam, R. Griessen, Phys. Rev. Lett. 102 (2009) 226102.

[1] Institute of Industrial Science, Univ. of Tokyo

3.4 Measurement of thin-film thicknesses grown on a Si substrate

K. Harada, T. Suemasu, K. Ito, D. Sekiba, S. Ishii, M. Matsumura, N. Takemoto

Introduction

Ferromagnetic silicide Fe_3Si is an attractive material for Si-based spintronics applications because the lattice parameter of Fe_3Si is 0.564 nm, nearly lattice-matching Si. Furthermore, Fe_3Si has a relatively high Curie temperature of approximately 803 K [1]. We have realized a small magnetoresistance (MR) ratio of 0.28% at room temperature (RT) in the $Fe_3Si/CaF_2/Fe_3Si$ magnetic tunnel junction (MTJ) structures [2]. To enhance the MR ratio, we deposited a Pt capping layer on the MTJs to prevent the oxidation of the top ferromagnetic layer in the MTJs. However, it is difficult to etch the Pt layer by wet etch process. Thus we decided to use the Ar^+ milling technique to etch the Pt layer. It is very important to get a precise etch rate of Pt. For that purpose, we adopted the RBS technique to evaluate the thickness of etched Pt, because the integrated intensity of RBS spectrum depends on the thickness of layers. In this article, we reported on the evaluation of etch rate of Pt layers by RBS measurement.

Experimental

The Pt (8 nm) was deposited at RT on a Si(111) substrate by electron-beam evaporation in a conventional MBE system. Then the samples were divided in four pieces and etched them by Ar^+ milling in the Nano-Processing Facility, supported by IBEC Innovation Platform, AIST. Table 1 shows the Ar^+ milling conditions. The etch time of four samples were varied as 0, 8, 12 and 20 s. The thickness of the etched layer was determined by RBS measurement at the C-course of Tadetron accelerator in UTTAC.

Table 1 Ar^+ milling conditions

Angle of ion radiation	Rotation	Flux	Back pressure	Ion beam
0° (perpendicular to samples)	12 rpm	5 sccm	4×10^{-2} Pa	298 V, 9.0 mA

Results and Conclusion

Figure 1 shows the RBS spectra of Pt/Si(111) samples after the Ar^+ milling was performed for different durations. The spectra of Pt were obtained clearly. A silver paste was used to fix the samples in the Ar^+ milling. That's why the signals of Ag appeared in Fig. 1. The etch rate was determined by the integrated intensity of RBS spectra of Pt. Figure 2 shows the etch rate of Pt. The etch rate was 1225 /s. It was found that the 8nm-thick Pt layer was completely removed by the Ar^+ milling for 39 s. It means that the etch rate of Pt was 0.20 nm/s. As a next step, we are going to adopt the same method for the Fe_3Si, CaF_2 and Fe thin films to determine their etch rates using Ar^+ milling so that we can process $Pt/Fe/Fe_3Si/CaF_2/Fe_3Si/CaF_2/Si(111)$ into mesa structures.

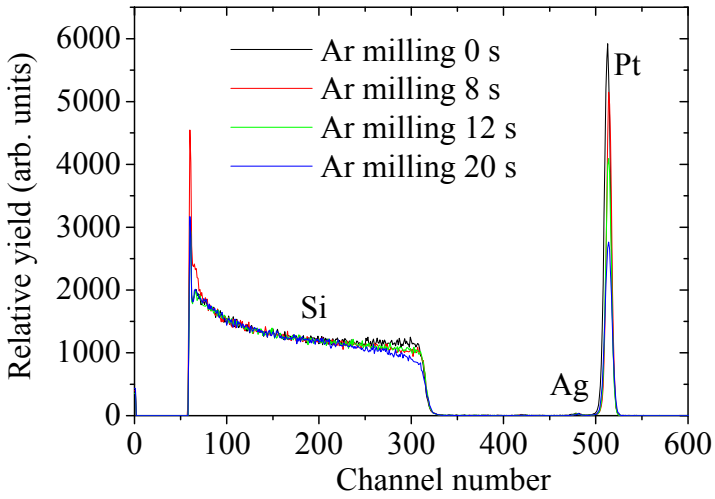

Fig. 1 RBS spectra of Pt/Si(111).

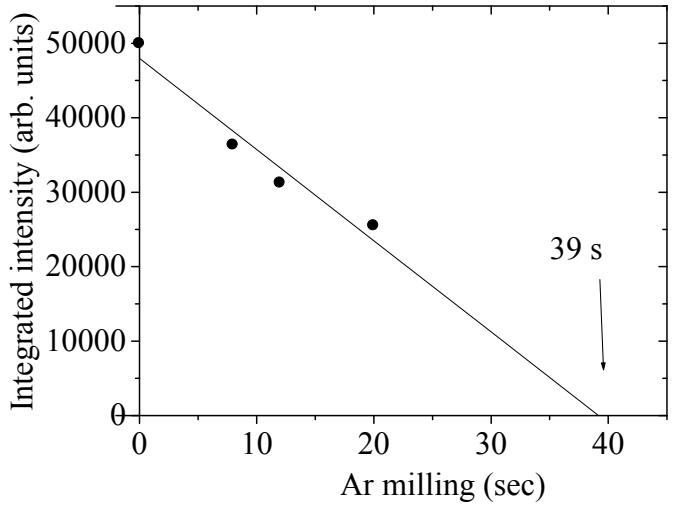

Fig. 2 Etch rate of Pt using Ar^+ milling.

Acknowledgements

This work was conducted at the Nano-Processing Facility, supported by IBEC Innovation Platform, AIST. The authors also thank the technical staffs of UTTAC for their supports during the experiment.

Reference

[1] A. Ionescu, C. A. F. Vaz, T. Trypiniotis, C. M. Gürtler, H. Garcia-Míquel, J. A. C. Bland, Phy. Rev. B **71**(2005)094401.

[2] K. Harada, K. S. Makabe, H. Akinaga, and T. Suemasu, J. Phys. Conference Series **266**(2011)012088.

3.5 Quantitative evaluation of nitrogen in perovskite oxynitride $SrTaO_{3-y}N_y$ thin films

D. Oka[1], Y. Hirose[1], K. Sasa, D. Sekiba, S. Ishii and T. Hasegawa[1]

Introduction

Perovskite oxynitrides $ABO_{3-y}N_y$ are a group of materials which possess both of oxygen and nitrogen ions on the same site of their structures The perovskite oxynitrides with many combinations of *A*-*B* cations have been mainly studied as non-toxic pigment or photocatalyst until now. On the other hand, they are also expected to be good candidates for new dielectic materials with unique property due to large covalency of metal-nitrogen bond and structural distortion, although there are only few reports about their dielectric property. For instance, it was reported that ceramics of $SrTaO_2N$ and $BaTaO_2N$ shows very high permittivity (ε) of ~3000 and ~5000, respectively, with low temperature coefficients [1]. However, it is difficult to synthesize densely sintered or single crystalline samples of perovskite oxynitrides required for reliable electrical capacitance measurements. One reason for this problem is that perovskite oxynitrides are decomposed at sintering temperature due to their very high melting points despite they are very stable in ambient atmosphere over 1000 ^oC. Another reason is the synthetic process of perovskite oxynitrides, where precursor oxides are nitrided by annealed under NH_3 flow at high temperature (~1000 ^oC). Since this reaction proceeds from the surface of the precursor materials, they must be fine powders in shape in order to accomplish perfect nitridation.

One solution for this problem is fabricating the materials in epitaxal thin film form. Kim *et al.* reported the dielectric property of a $BaTaO_{3-x}N_x$ thin film epitaxially grown by pulsed laser deposition (PLD) method [2]. Their $BaTaO_{3-x}N_x$ epitaxial thin film showed paraelectric property with small temperature coefficient as likely as the ceramic $BaTaO_2N$ sample. However, its ε of ~220 is about 1/20 smaller than the value of the ceramic. Moreover, they didn't determine the nitrogen content of their film despite its importance. We suggested that this is mainly due to the difficulty of quantitative evaluation of light elements including nitrogen in thin film materials. In this study, therefore, we determined the nitrogen contents of epitaxial thin films of a perovskite oxynitride $SrTaO_{3-y}N_y$ by nuclear reaction anarysis (NRA) in order to reveal intrinsic dielectric property of the perovskite oxynitrides with well-characterized nitrogen contents.

Experimental

$SrTaO_{3-y}N_y$ films were epitaxially grown on (100) plane of $SrTiO_3$ (STO) single crystalline substrates by nitrogen-plasma assisted PLD method. A sintered pellet of $Sr_2Ta_2O_7$ was ablated by a KrF excimer laser (λ = 248 nm) under the mixture of nitrogen molecules and radicals supplied from an electron cyclotron resonance plasma atom source. The nitrogen amount (y) in $SrTaO_{3-y}N_y$ films was controlled with growth parameters such as temperature of substrates (T_s), partial pressure of nitrogen gas (P_{N2}), and repetition rate (R_L) and energy (E_L) of the excimer laser. Eepitaxial growth of the perovskite $SrTaO_{3-y}N_y$ was confirmed

[1] Department of Chemistry, The University of Tokyo, 7-3-1 Hongo, Bunkyo-ku, Tokyo 113-0033, Japan

by X-ray diffraction (XRD) measurements.

The nitrogen contents in the films were evaluated by NRA method using $^{15}N(p,\alpha\gamma)^{12}C$ reaction based on the assumption that $^{15}N/^{14}N$ ratio in the obtained films are the same as the natural isotope ratio. We chose the resonance peak at 902 keV for excitation and detected the emitted γ-ray with $Bi_4Ge_3O_{12}$ (BGO) scintillation counters. A TiN epitaxial thin film was used as a standard sample. Measurements were done on the course D of 1MV tandetron at UTTAC.

Result and Discussion

Fig. 1 shows the nitrogen contents in the $SrTaO_{3-y}N_y$ films fabricated with various growth parameters. The nitrogen contents show the following trends: y is almost independent of T_s, while it is highly sensitive to the change of P_{N2}, showing the largest value at 1.0 x 10^{-5} Torr. The repetition rate R_L and pulse energy of the excimer laser E_L also have great impact on y, namely, y increases with decrease of R_L and E_L. These results indicate that nitrogen content y increases under the condition where the supply of N radical from ECR atom source becomes larger compared with that of other source elements from ablated target. Independency of y on T_s indicates that the T_s is too low for the cleavage of stable N_2 molecules and only the N radicals contribute the reaction.

Fig. 2 shows the lattice constants of the $SrTaO_{3-y}N_y$ thin films with various y values determined by XRD measurements. The crystal structures are tetragonally distorted (lattice constant $c > a$) and both a and c values linearly become larger with increase of y. This result can be explained by the fact that N^{3-} ion (R = 1.46 Å) is larger than an O^{2-} ion (R = 1.36 Å).

References

[1] Young-Il Kim, Patrick M. Woodward, Karim Z. Baba-Kishi, and Cheuk W. Tai, Chemistry Of Materials **16**, 1267-1276 (2004).

[2] Young-Il Kim, Weidong Si, Patrick M. Woodward, Eli Sutter, Sangmoon Park, and Thomas Vogt, Chemistry Of Materials **19**, 618-623 (2007).

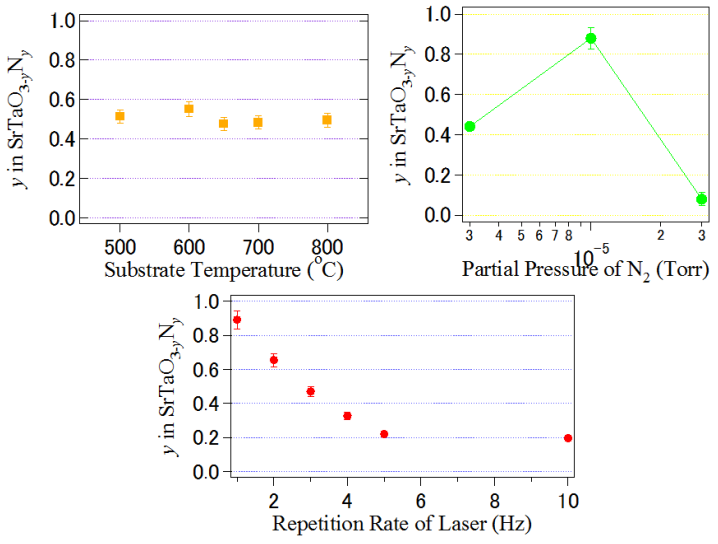

Fig. 1. Nitrogen contents y in the $SrTaO_{3-y}N_y$ films grown under various conditions evaluated by the NRA method.

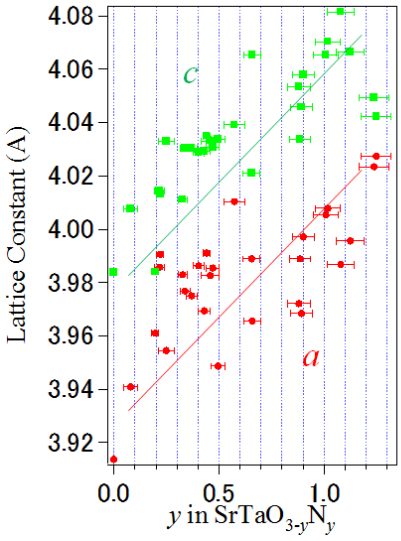

Fig. 2. Lattice constants of $SrTaO_{3-y}N_y$ with different y.

3.6 Strong correlation between nucleation rate in $N_2/H_2O/SO_2$ and consumption of SO_2 under irradiation of 20 MeV protons

S.Tomita, H. Tanikawa, S. Funada, H. Kobara[1], Y. Nakai[2], and K. Sasa,

The possible correlation between solar activities and global environment attracts attentions in connection with global warming [1]. One of possible mechanisms proposed for the correlation is the formation of nano-particles due to high energy charged particles, i.e. cosmic rays. Cosmic rays ionize atmospheric gases, and the ions are believed to play important roles for the formation of aerosols in the atmosphere. One of the roles is oxidation of SO_2, and the other is ion induced nucleation. In order to investigate these processes, we irradiated gas mixture of $N_2/H_2O/SO_2$ at atmospheric pressure with 20 MeV protons, and measured both generated droplet density and the consumption of SO_2 as a function of beam intensity.

Experiments were conducted with 12UD Pelletron. The concentration of SO_2 in the sample gas was fixed to 100ppb, and the relative humidity was 30% at room temperature. The generated droplets were measured by a differential mobility analyzer [2], and the concentration of SO_2 were monitored with a pulsed fluorescence gas analyzer (Thermo 43S). A typical result of SO_2 concentration is shown in Fig.1 together with the intensity of 20 MeV protons. It is clearly seen that the concentration decreases during proton irradiation. The consumption of SO_2 in the sample gas is mainly due to the oxidation with OH radicals formed by high energy protons. In Fig. 2, the consumption is plotted together with the density of droplet generated by the irradiation as a function of beam intensity. Both results show similar trend, which implies the importance of oxidation process of SO_2.

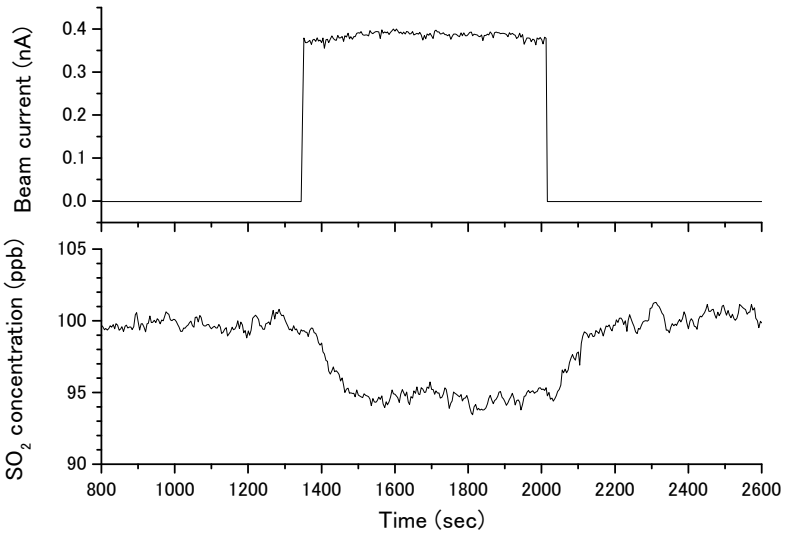

Fig. 1: SO_2 concentration (lower frame) and beam intensity of 20MeV protons on sample gas ($N_2/H_2O/SO_2$). The concentration of SO_2 was 100ppb, and relative humidity was 30% at room temperature.

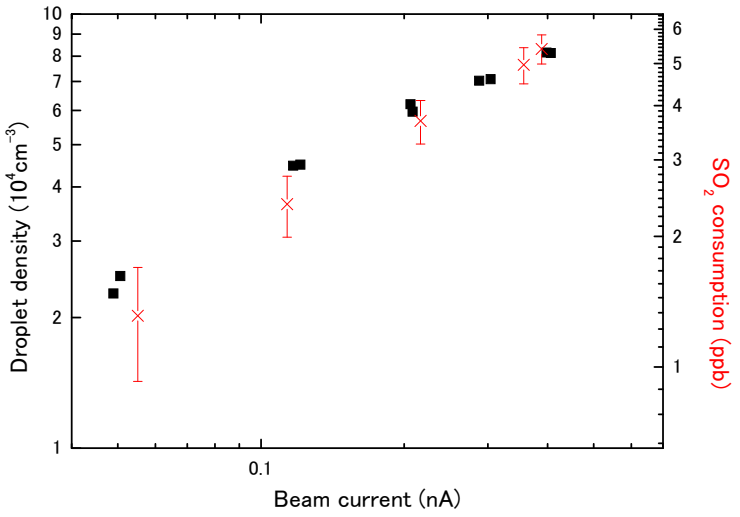

Fig. 2: SO_2 consumption (crosses) and generated droplet density (squares) as a function of beam intensity of 20 MeV .proton.

References

[1] Carslaw, K.S., R.G. Harrison, and J. Kirkby, Science, 2002. **298**(5599): p. 1732-1737.

[2] Seto, T., et al., Journal of Aerosol Science, 1997. **28**(2): p. 193-206.

[1] National Institute of Advanced Industrial Science and Technology, Onogawa 16-1, Tsukuba, Ibaraki 3058569, Japan

[2] RIKEN Nishina Center, Radioactive Isotope Laboratory, Wako, Saitama 3510198, Japan

3.7 Rutherford backscattering of potassium intercalated graphite

T. Kondo, J. Oh, D. Guo, T. Suzuki, K. Arakawa, T. Machida, T. Shikano, Y. Saito, K. Iwatake, S. Ishii, D. Sekiba, H. Kudo and J. Nakamura

To characterize the amount and intercalation feature of potassium atoms on graphite, we have applied ex-situ RBS (Rutherford backscattering) technique for the surface of HOPG (Highly oriented pyrorytic graphite) with potassium deposited at room temperature in UHV (ultra-high vacuum). The observed typical RBS spectrum is shown in Fig. 1(a). With a large backscattering intensity component below 0.37 MeV, there is a peak at around 1.08 MeV. Each peak component has been identified as to correspond to carbon and potassium, respectively, based on the following RBS equation:

$$E_1 = \left(\frac{M_1 \cos\theta + \sqrt{M_2^{\,2} - M_1^{\,2} \sin_2 \theta}}{M_1 + M_2} \right)^2 E_0 \quad ,$$

where E_1 is the ion energy scattered from the sample, E_0 the incident He ion energy (1.6 MeV), M_1 the atomic mass of incident ion (4 amu), M_2 the atomic mass of sample and θ the angle of solid state detector (150 degree). From the peak intensity ratio between carbon and potassium, the amount of potassium can be roughly estimated as 1.1 ML, where 1 ML is defined as the amount of potassium atoms with the same number of carbon atoms at the top-most graphene layer on graphite. The peak component of potassium is limited at around 1.08 MeV, more precisely from 1.05 to 1.1 MeV. This indicates that potassium atoms locate near the surface of graphite and not deeply intercalated into the bulk of graphite. According to the literature, the potassium atoms were reported to intercalate into graphite by layer-by-layer manner at room temperature based on the LEED (low energy electron diffraction) analysis [1]. The result in Fig. 1(a) seems to agree with this conclusion. However, it is not clear whether the potassium located “on” the top-most graphene layer or “below” the layer from Fig. 1(a) because the width of the peak is not clear to distinguish the effect of the finite energy resolution of RBS in this particular case. Further examination with enough signal-to-noise ratio and/or high resolution RBS is required to clarify this point.

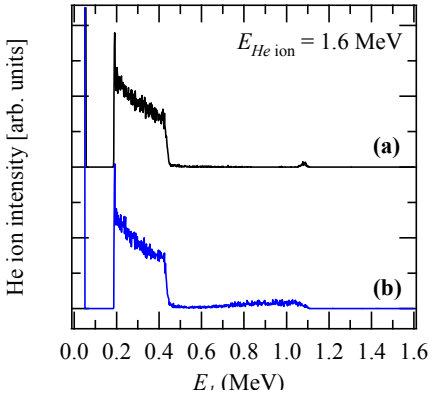

Fig. 1 RBS of K/HOPG, (a) as-deposited at RT, (b) with heating to 800 K

Fig. 1(b) shows the RBS spectrum of graphite with potassium deposited in UHV at room temperature followed by heating to ~800 K. Contrary to the case of Fig. 1(a) there is a wide peak component below 1.08 MeV. The component is considered to be due to the intercalated potassium in the bulk of graphite. The deepest depth and total amount of potassium can roughly be estimated as >0.5 μm and > 14 ML, respectively. Since the largest intensity of the component does not positioned at 1.08 MeV, potassium density is considered to be not uniform near the surface of graphite. Further investigation is required to clarify the density profile of potassium in detail.

Reference

[1] N. J. Wu and A. Ignatiev, Phys. Rev. B, **28** (1983) 7288.

4.

ACCELERATOR MASS SPECTROMETRY

4.1 A preliminary measurement of cosmogenic ^{36}Cl in the Greenland NEEM ice core

K. Sasa, K. Kurosumi, Y. Matsushi[1], Y. Tosaki[2], T. Takahashi, K. Sueki, N. Kinoshita, K. Horiuchi[3], H. Matsuzaki[4] and K. Azuma[5]

The North Greenland Eemian Ice Drilling - NEEM - is an international ice core research project aimed at retrieving an ice core from North-West Greenland (77.45°N, 51.06°W). The NEEM project commenced in 2007 and has the goal of retrieving an undisturbed record of the full Eemian interglacial period 115,000 - 130,000 years ago [1]. We have been engaged in a collaborative research project to measure cosmogenic ^{36}Cl in the NEEM ice core. We have attempted to help with the dating by investigating ^{10}Be/^{36}Cl ratios. There are two aspects. 1) To measure ^{10}Be/^{36}Cl in the deepest ice as a dating exercise, and 2) to measure ^{10}Be/^{36}Cl in several periods below 2200 m where the ice seems disturbed, to try to identify inclusions of older ice or overturned ice. There are five episodes of rapidly changing δ^{18}O values in the NEEM ice core.

We used sawdust samples for trial measurements of ^{36}Cl in the NEEM ice core. In addition, ^{10}Be in the NEEM ice core has been measured at Uppsala University. Isotope dilution method was attempted to estimate natural Cl content in the ice [2]. A sodium chloride-35 powder from Aldrich Co. (^{35}Cl purity: 99.9 at. %) was used as the carrier. Ice samples and chemical blanks were spiked with 0.8 mg Cl of the ^{35}Cl-enriched carrier. Chemical blank was also spiked with 0.5 mg of a normal Cl carrier, so that it works also as a standard with a known content of initial Cl with natural isotope ratio. Table 1 shows a preliminary result of ^{36}Cl trial measurements in the NEEM ice core.

Table 1. Preliminary result of ^{36}Cl trial measurements in the NEEM ice core.

Sample no.	Depth (m)	Age (ka)	^{36}Cl/Cl (10^{-15})	^{35}Cl/^{37}Cl	^{36}Cl concentration (10^3 atoms/g)
2385 - 2390	1315	9.65	59 ± 7	103	2.30 ± 0.13
2847 - 2852	1567	19.3	140 ± 4	33	5.37 ± 0.24
Blank 1			6.4 ± 0.9	9.1	
Blank 2			6.0 ± 0.7	9.1	

Acknowledgements

This work is supported in part by the Grants-in-Aid for Scientific Research Programs of the Ministry of Education, Culture, Sports, Science and Technology, Japan (Grants-in-Aid No. 21310004 and 22241003).

References

[1] Buchardt, Susanne L., Dahl-Jensen, Dorthe, *Annals of Glaciology*, Vo. 48, 1, 2008, 100-102(3).

[2] Y. Matsushi et al., *Nucl. Instr. and Meth. B*, 268 (2010) 1205-1208.

[1] Disaster Prevention Research Institute, Kyoto University
[2] Geological Survey of Japan, National Institute of Advanced Industrial Science and Technology (AIST)
[3] Hirosaki University
[4] MALT, The University of Tokyo
[5] National Institute of Polar Research

4.2 Groundwater ages in the volcanic aquifers of Mt. Fuji, central Japan

Y. Tosaki[1], N. Tase, K. Sasa, T. Takahashi, S. Gmati and S. Ueno

Introduction

In areas closely related to Quaternary volcanoes, groundwater is a major source of water used for drinking, agricultural, and industrial purposes. Because the surface of these volcanoes is generally overlain by high-porosity volcanic sediments, the resulting high permeability allows them to contain large reservoirs of groundwater. An understanding of groundwater flow systems and groundwater age is therefore an important component of the sustainable management of the groundwater resources in volcanic areas.

In our previous work [1], we proposed a methodology for estimating groundwater age based on the ^{36}Cl bomb-pulse. The spatial distribution of ^{36}Cl-based residence times for springs around Mt. Fuji, central Japan was basically consistent with that of tritium-based estimates calculated from data presented in previous studies. However, the estimated residence times were not in agreement between the two tracers, showing an overestimation for ^{36}Cl.

To further examine the applicability of bomb-derived ^{36}Cl in dating young groundwater, this study focuses on the older, deeper groundwater in the southern foot of Mt. Fuji. The distinctive difference in the elemental compositions of the Older Fuji and Younger Fuji volcanic rocks yields contrasting chemical composition of groundwater in each aquifer. In conjunction with the altitude effect on stable isotopic composition of oxygen, our results provided insights into the sources of the pumped groundwaters and their ages.

Study site and methods

During sampling campaigns conducted between July 2007 and January 2010, groundwater samples were obtained from municipal and private water supply wells on the southern foot of Mt. Fuji. The surface geology is dominated by lava flows of the Younger Fuji volcano, partly overlain by alluvial deposits. In some locations, the underlying Older Fuji deposits are exposed on the surface. Most of the wells are screened in both of shallow (i.e. Younger Fuji lava flows and/or alluvial deposits) and deep (i.e. Older Fuji mudflow deposits) aquifers (see [1] for detailed geology).

Bicarbonate (HCO_3^-) concentrations were determined by titration with dilute H_2SO_4 solution. Other major dissolved ions (Na^+, K^+, Mg^{2+}, Ca^{2+}, Cl^-, SO_4^{2-}, and NO_3^-) were measured by ion chromatography analysis (Ion Analyzer IA-100; Dkk-Toa) at UTTAC. Stable isotope ratios of oxygen ($\delta^{18}O$) were analyzed with a stable isotope mass spectrometer (MAT252; Thermo Finnigan) at the Hydrology Lab, Graduate School of Life and Environmental Sciences, University of Tsukuba (analytical error 0.1‰). After standard chemical processing [2], the samples with NO_3^- concentrations smaller than approximately 10 mg/L were measured for $^{36}Cl/Cl$ ratios with the AMS system at UTTAC.

[1] Geological Survey of Japan, National Institute of Advanced Industrial Science and Technology (AIST)

Results and discussion

Figure 1(a) presents the relationship between K^+/Na^+ molar ratios and $\delta^{18}O$ values of the groundwater samples. The occurrence of a strong correlation between the two parameters clearly indicates the presence of two end-member components mixing in the sampled wells through the screens. Because the Older Fuji deposits are characterized by the high content of Na relative to K [3], one component with low K^+/Na^+ ratio and low $\delta^{18}O$ value would correspond to the groundwater in the deep Older Fuji aquifers, which should have a high recharge elevation. The other with higher $\delta^{18}O$ value (i.e. lower recharge elevation) may originate from the Younger Fuji and/or shallow alluvial aquifers.

From the measured $^{36}Cl/Cl$ ratios given in Figure 1(b), two samples with low $\delta^{18}O$ value show remarkably low $^{36}Cl/Cl$ ratios around 30×10^{-15}. The remaining samples have varying $^{36}Cl/Cl$ ratios from ~100×10^{-15} to ~800×10^{-15}, which are obviously higher than those of the above-mentioned two samples probably due to the addition of bomb-derived ^{36}Cl. The wide range of $^{36}Cl/Cl$ ratios for these samples may indicate the existence of multiple components for the low $\delta^{18}O$ end-member, possibly originating from the Younger Fuji and alluvial aquifers.

Based on our results, the groundwater in the Older Fuji aquifer was recharged during the pre-bomb period (i.e. >60 years ago). Contrastingly, the groundwater ages in the Younger Fuji and alluvial aquifers are estimated to be approximately 30–50 years. To provide more quantitative estimates of the groundwater ages, further studies will involve the application of "^{36}Cl bomb-pulse dating" proposed previously [1].

References

[1] Y. Tosaki et al., Ground Water (2011) in press, doi:10.1111/j.1745-6584.2010.00795.x.

[2] Y. Tosaki et al., Water 3 (2011) 64.

[3] K. Ikeda, Bull. Geol. Surv. Japan 40 (1989) 331.

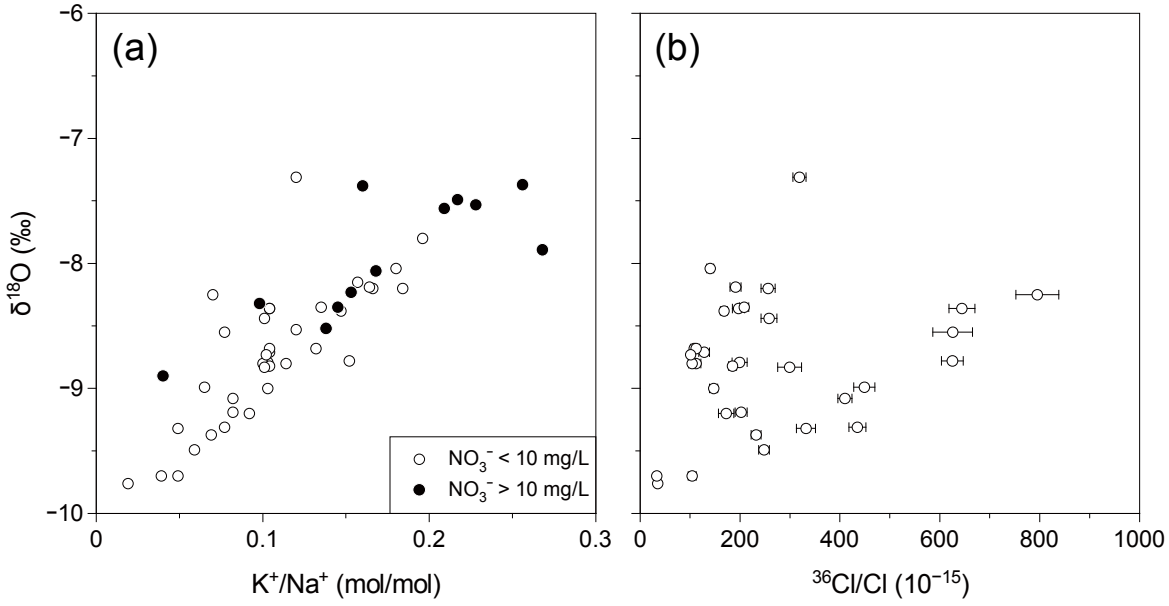

Figure 1. (a) Relationship between K^+/Na^+ molar ratios and $\delta^{18}O$ values of groundwater. (b) Relationship between $^{36}Cl/Cl$ ratios and $\delta^{18}O$ values.

4.3 AMS study of ^{36}Cl in meteorites

Y. Oura[1], Y. Sasaki[1], Y. Hamanaka[1], K. Sasa, T. Takahashi, K. Sueki, N. Kinoshita, T. Amano, J. Kitagawa, K. Kurosumi, M. Matsumura.

The research group led by M. Honda have been measuring some cosmogenic nuclides in a lot of fragments of Gibeon meteorites to be clear the depth dependence of cosmogenic nuclide contents. The concentrations of these nuclides vary by 5 orders of magnitude from fragment to fragment, and systematic correlations among cosmogenic nuclides are observed [1]. ^{45}Sc among cosmogenic nuclides produced in an iron meteorite are stable nuclides and Sc element consists of a unique nuclide, ^{45}Sc, in nature. Sc is classified to geochemical lithophile element, thus non-cosmogenic original Sc contents in iron meteorite is supposed to be very low and its concentration is very interesting for solving a process of a internal core of planet. We have to analyze a fragment with ultra trace of cosmogenic nuclide content to reduce their contribution. So ^{36}Cl contents were determined in a fragment of Gibeon and Campo del Cielo, which we got recently, to find its degree of cosmogenic nuclide contents and to evaluate if the fragment is good for analysis. And a content of cosmogenic nuclides other than ^{45}Sc is helpful for evaluation of contamination of terrestrial ^{45}Sc in its determination. About 1 g of a piece cut from each fragment was subjected to analysis. Two pieces were obtained from a fragment of Campo del Cielo. The ^{36}Cl content was found to be 0.019 ± 0.001 dpm/kg in Gibeon and 2.38 ± 0.01 and 2.30 ± 0.01 dpm/kg in Campo del Cielo. Observed ^{36}Cl contents in Gibeon by Honda et al. were varied from 0.003 to 5.05 dpm/kg. Our fragment of Gibeon is classified to low cosmogenic nuclide content group and it is estimated that the fragment of Gibeon was located in relatively deep inside of the meteoroid. On the contrary Campo del Cielo fragment was located closer to the surface and ^{45}Sc in it was predicted to be mostly cosmogenic origin.

AMS group in University of Tsukuba are developing a technique of ^{41}Ca analysis. We have a plan of application of ^{41}Ca to meteorites. There is no standard reference material with certified value of ^{41}Ca concentration, thus correlation between ^{41}Ca and other cosmogenic nuclide is one of way of evaluation of determined ^{41}Ca concentration value. In Fig.1, the correlation between ^{41}Ca and ^{36}Cl production rates in iron meteorite with different meteoroid radius based on a model calculation by Ammon et al. [2] are shown. No systematic difference among different radii is observed and 0.028 and 3.0 dpm/kg of ^{41}Ca are expected to be determined in Gibeon and Campo del Cielo, respectively, according to the correlation.

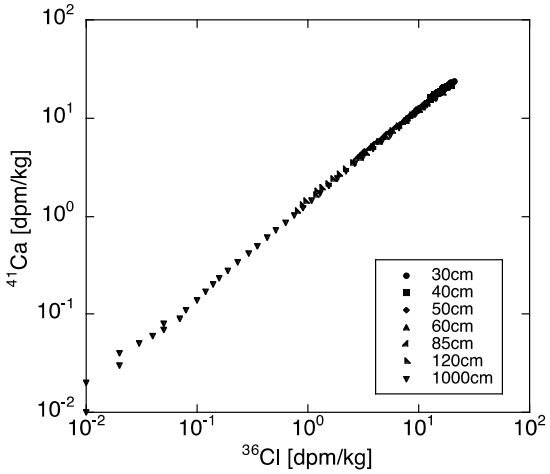

Fig.1 Correlation between ^{41}Ca and ^{36}Cl in iron meteorites based on model calculation [2].

[1]Graduate School of Science and Engineering, Tokyo Metropolitan University

References

[1] M. Honda, N. Nagai, K. Nagao, K. Bajo, N. Takaoka, Y. Oura, K. Nishiizumi, *J. Phys. Soc. Jpn.* **78** Suppl. A (2009) 12.

[2] K. Ammon, J. Masarik, I. Leya, *Meteorit. Planet. Sci*. **44** (2009) 485.

5.

INTERDISCIPLINARY RESEARCH

5.1 Acceleration energy dependence of nanohole sizes formed by ion irradiation and following HF etching in thermally grown SiO_2 films

M. Fujimaki[1], K. Awazu[1], T. Komatsubara

A biomolecular sensor utilizing waveguide modes (WM) is one of the promising sensors for molecular adsorption detection [1, 2]. We have developed a WM sensor that used a sensing plate having a multilayer structure consisting of a SiO_2 glass substrate, a single-crystalline Si layer, and a thermally grown SiO_2 glass waveguide. We named the sensing plate 'monolithic sensing plate' [3]. The monolithic sensing plate illuminated under the Kretschmann configuration operates as a sensor that is capable of detecting modifications in the dielectric environment near the waveguide surface by measuring change in reflectivity. Figure 1 shows an optical set-up of the sensor, in which a spectral readout system is used. In the system, collimated white light is irradiated to the monolithic sensing plate placed on the bottom of a prism and a spectrum of the reflected light is observed by a spectrophotometer. We reported that significant enhancement of sensitivity of the WM sensor was achieved by perforating the SiO_2 waveguide, in which selective etching of latent tracks formed in the waveguide by ion irradiation was used [3, 4]. In the present research, we investigated optimal ion irradiation conditions to form desirable nanoholes.

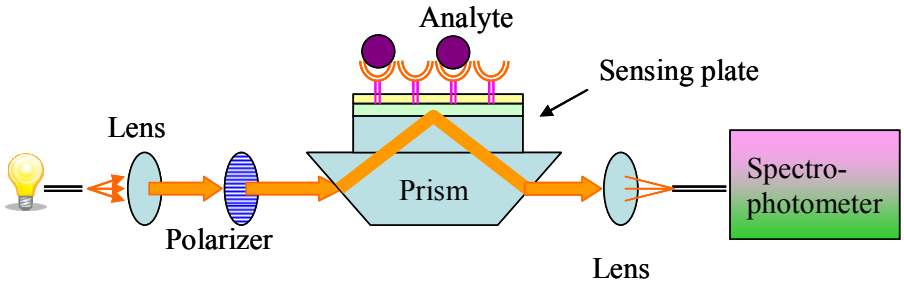

Fig.1. Optical set-up of the WM sensor, in which the monolithic sensing plate is used

The substrate used was a Si substrate having a 2-μm-thick thermally grown SiO_2 layer on its surface. For perforating the SiO_2 layer, ion irradiation and etching by 5% HF solution following the irradiation were applied to the layer. Ion irradiation was performed using the 12 UD Pelletron tandem accelerator at the University of Tsukuba. Irradiated ions were Au, Br, and Cl ions. The irradiated substrate was dipped in the HF solution for 2 min. Fabricated nanoholes were observed using a scanning electron microscope (SEM, Hitachi High-Technologies, S4800). Figures 2a, 2b, and 2c respectively show the SEM images of the perforated surfaces formed by the Au, Br, and Cl-ion irradiation and the following HF etching. The acceleration energy of each ion is shown in the images. As can be seen in Figs. 2a and 2b, good-shaped nanoholes are observed in all the cases of the Au and Br-ion irradiation, and the diameters of the nanoholes scarcely depend on the irradiation conditions, indicating that acceleration energy of 34.5 MeV is enough for Au ions to form desirable nanoholes and that of 25.0 MeV for Br ions. The projected range of Au ions accelerated with 34.5 MeV and that of Br ions with 25.0 MeV are ~8 μm. This value is much

larger than the thickness of the waveguide of the monolithic sensing plate, where a typical thickness of the waveguide is ~500 nm. This means that these ions go through the waveguide layer and that the formed nanoholes penetrate the waveguide layer.

In the case of the Cl-ion irradiation, formation of nanoholes was not observed under the irradiation of 66.4-MeV Cl ions, whereas nanoholes were formed under the conditions with smaller acceleration energy. The nanohole with the largest diameter was created by the irradiation of Cl ions accelerated with 16.5 MeV. This result is consistent with the previous reports [5, 6].

The obtained information is useful to realize a low-cost and high-productivity fabrication process of the perforated monolithic sensing plate.

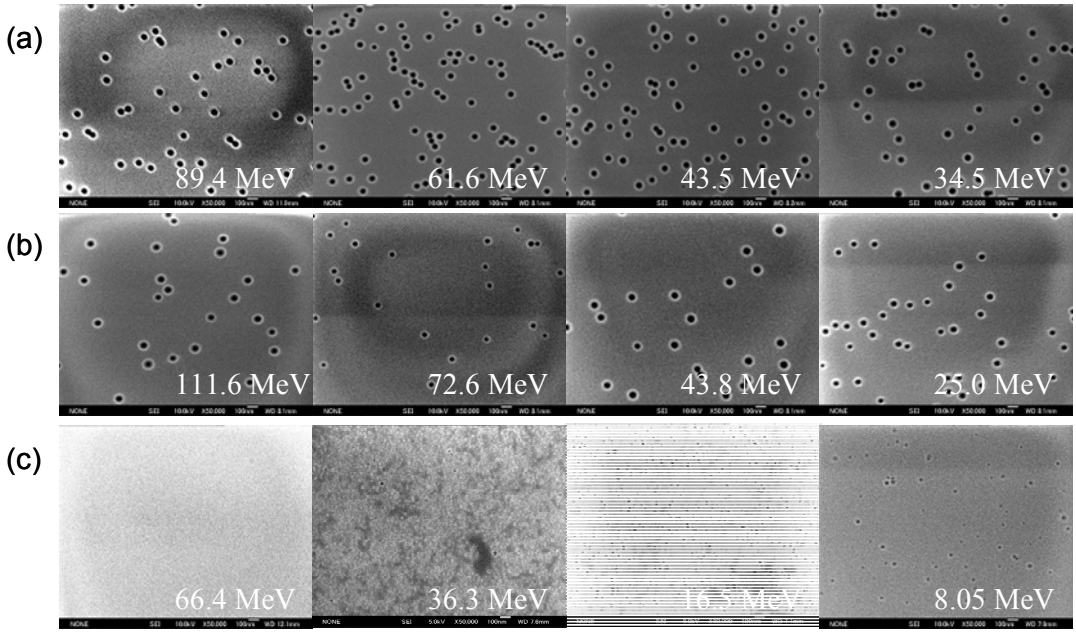

Fig.2. SEM images of the perforated surfaces formed by the Au (a), Br (b), and Cl (c) ion irradiation and the following HF etching.

This study was supported by Industrial Technology Research Grant Program in 2009 from New Energy and Industrial Technology Development Organization (NEDO) in Japan.

References

[1] W. Knoll, MRS Bulletin **16** (1991) 29.

[2] M. Fujimaki et al., Nanotechnology **19** (2008) 095503.

[3] M. Fujimaki et al., Opt. Express **16** (2008) 6408.

[4] K. Awazu et al., Opt. Express **15** (2007) 2592.

[5] J. Jensen et al., Nucl. Instrum. Methods Phys. Res. B **243**, 119 (2006).

[6] K. Nomura et al., Nucl. Instrum. Methods Phys. Res. B (in press).

[1] National Institute of Advanced Industrial Science and Technology (AIST)

5.2 PIXE analyses of trace Ti in single fluid inclusions in quartz from Tsushima granite

M. Kurosawa, S. Ishii and K. Sasa

Introduction

Titanium oxides and silicates have very limited solubility in water, so that Ti is thought to be essentially immobile by crustal fluids at igneous and metamorphic conditions. Based on the immobility, Ti contents in igneous and metamorphic rocks are often used as an indicator of the origin and formation process. On the other hand, titanium minerals formed by fluid reactions are frequently observed in metamorphic and hydrothermal-alteration rocks. Recent hydrothermal experiments have also shown the extreme high solubility in chloride and fluoride-rich solutions at high-pressure conditions [1]. Thus, fluid transport of Ti in geological environments has attracted attention as a source of the titanium mineral formation. A part of geological fluids is normally trapped as fluid inclusions inside minerals during transportation in rocks, so that fluid inclusions are expected as an information source about the Ti transportation and fluid chemistries. Trace amounts of Ti have been sometimes detected for fluid inclusion analyses by PIXE and synchrotron X-ray fluorescence [2, 3]. The concentrations and behaviors, however, have not been fully understood. For these reasons, we determined trace-element compositions of single fluid inclusions in quartz from Tsushima granite by using micro-PIXE.

Sample

Tsushima granite, Nagasaki prefecture, is typical calc-alkaline Miocene granite in Japan and contains abundant miarolitic cavities [4]. The emplacement level estimated is 2–6 km deep. Quartz in the granite and cavities contains many polyphase and vapor-rich fluid inclusions formed by brine-vapor separation due to fluid boiling (Fig. 1). Two-phase aqueous inclusions are also found. Thus, we analyzed the three types of inclusions. Salinities of the polyphase inclusions were of 28–55 wt.% NaCl eq. and the homogenizing temperatures (Th) ranged from 782 to 250 °C. The two-phase inclusions showed Th of 220–521 °C. Measured inclusions were typically 50 μm in size, ellipsoidal or negative-crystal shapes, and the inclusion depths were less than 10 μm.

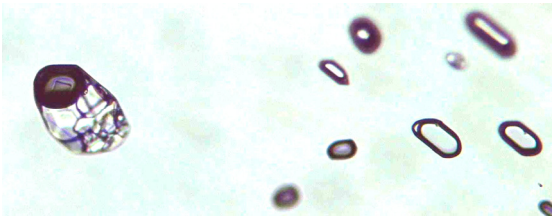

Fig.1. Photomicrograph of polyphase and vapor-rich fluid inclusions in a quartz crystal from miarolitic cavity at Tsushima granite. A large inclusion of the left side is a polyphase inclusion, 70 μm in size, with a bubble (dark ellipsoidal) and many daughter crystals of halite, calcite and so on. Several ellipsoids in the right side are vapor-rich inclusions.

Experimental

PIXE analyses were performed at the 1MV Tandetron. A 1.0 to 5.0 nA beam of 1.92-MeV proton was focused to a ~50 x 50 μm spot on the sample. The beam incidence was normal to the sample surface, and

the X-ray measurement take-off angle was 45˚. The characteristic X-rays were collected by the Si(Li) X-ray-energy detector with a nominal resolution of 153 eV at 5.9 keV. A 55-μm-thick Mylar film was used to attenuate the intense X-rays from the predominant light elements. All samples were analyzed to the integrated charges of 0.5 to 5.0 μC. Quantification was performed based on the ellipsoidal-inclusion calculation model, and the total analytical errors for trace elements were estimated to be of ±11- 40 % [5].

Results and Discussion

Typical PIXE spectra of the inclusions consisted of K X-ray peaks from Cl, K, Ca, Ti, Mn, Fe, Cu, Zn, Ge, Br, Rb, and Sr, and L X-ray peaks from Pb and Ba. The peaks from Ti are adjacent to those from Ba, so the Ti peaks are conspicuous for the vapor-rich inclusions with low Ba contents. Contents of Ti determined were of 100–600 ppm for polyphase and vapor-rich inclusions, and 2–50 ppm for the two-phase inclusions, respectively. The almost same contents in the polyphase and vapor-rich inclusions imply that apparent partition coefficients of Ti between vapor and brine ($D_{vapor/brine}$) during fluid boiling are nearly unity. The value is relatively larger than those expected, and the enrichment into vapor phase may also be supposed. The contents of Ti were also strongly positively correlated with Cl contents (Fig. 2), suggesting transportation of Ti as chlorine complex in hydrothermal fluids. The result is consistent with the high solubility of Ti in saline water [1]. In addition, the correlations between Cl and Ti showed distinctive trends among the inclusion types. These distinctive trends are thought to reflect changes of process or pressure and temperature conditions at the fluid formation. Ti contents also show frequently correlation with contents of K, Ca, Fe, Sr, and Ba. In the cavities, small amounts of titanite ($CaTiSiO_5$) and ilmenite ($FeTiO_3$) are present coexisting with K-feldspar ($KAlSi_3O_8$), so the same behavior of Ti with Ca, Fe, and K can be understood. The behavior of Sr and Ba are similar to those of Ca and K in granite systems, respectively, so their correlation with Ti may be reasonable.

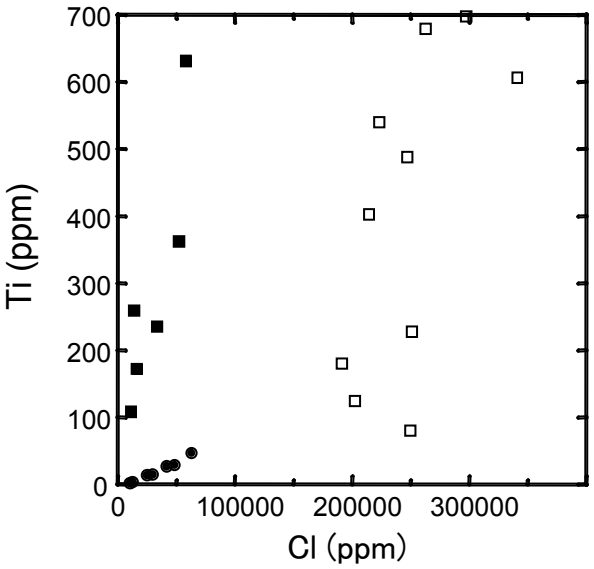

Fig.2. Elemental correlation between Cl and Ti in fluid inclusions from miarolitic cavities at Tsushima granite. Open square: polyphase inclusion; solid square: vapor-rich inclusion; solid circle: two-phase inclusion.

References

[1] J. F. Rapp et al., Geology, 38 (2011) 323.

[2] A. J. Anderson et al., Can. Mineral., 36 (1998), 511.

[3] B. Ménez et al., Geochim. Cosmochim. Acta, 66 (2002), 561.

[4] K. C. Shin et al., Res. Geol., 59 (2009), 25.

[5] M. Kurosawa et al., Nucl. Instr. Meth., B266 (2008), 3633.

6. LIST OF PUBLICATIONS

The publications listed here are those released in the fiscal year 2010 by all the workers listed on p.60.

6.1 Journals

ACCELERATOR AND EXPERIMENTAL FACILITIES

1. K. Sasa, T. Takahashi, Y. Nagashima, Y. Tosaki, N. Kinoshita, K. Sueki, H. Matsumura, K. Bessho, Y. Matsushi, Accelerator mass spectrometry at the tsukuba 12 MV pelletron tandem accelerator, Proceedings of IPAC'10, Kyoto, Japan, Joint Accelerator Conference Website (JACoW), 223-225 (2010).

2. T.Moriguchi, S.Ishimoto, S.Igarashi, A.Ozawa, Y.Abe, Y.Ishibashi, Y.Ito, H.Ooishi, H.Suzuki, M.Takechi, K.Tanaka, Developments of a thick and large solid hydrogen target for radioisotope beams, Nuclear Instruments and Methods in Physics Research A, 624 (2010) 27.

NUCLEAR PHYSICS

3. K. Setoodehnia, A. A. Chen, T. Komatsubara, S. Kubono, D. N. Binh, J. F. Carpino, J. Chen, T. Hashimoto, T. Hayakawa, Y. Ishibashi, Y. Ito, D. Kahl, T. Moriguchi, H. Ooishi, A. Ozawa, T. Shizuma, Y. Sugiyama, and H. Yamaguchi, Spins and parities of astrophysically important ^{30}S states from ^{28}Si(^{3}He, nγ)^{30}S, Phys. Rev. C 83, 018803 (2011) [4 pages]

4. A. Kim, N.H. Lee, I.S. Hahn, J.S. Yoo, M.H. Han, S. Kubono, H. Yamaguchi, S. Hayakawa, Y. Wakabayashi, D. Binh, H. Hashimoto, T. Kawabata, D. Kahl, Y. Kurihara, Y.K. Kwon, T. Teranishi, S. Kato, T. Komatsubara, B. Guo, G. Bing, W. Liu, Y. Wang, Direct measurement of the ^{14}O(alpha,alpha)^{14}O cross section for astrophysically important ^{14}O + alpha resonances, Journal of the Korean Physical Society, Vol. 57, No. 1, July (2010), pp. 40-43

5. A. Ozawa, Studies of nuclear structure for unstable nuclei by RI beams, Genshikaku-Kenkyu Vol. 54, 14-23, (2010), (Japanese)

6. B.Sun, R.Knöbel, H.Geissel, Yu.A.Litvinov, P.M.Walker, K.Blaum, F.Bosch, D.Boutin, C.Brandau, L.Chen, I.J.Cullen, A.Dolinskii, B.Fabian, M.Hausmann, C.Kozhuharov, J.Kurcewicz, S.A.Litvinov, Z.Liu, M.Mazzocco, J.Meng, F.Montes, G.Münzenberg, A.Musumarra, S.Nakajima, C.Nociforo, F.Nolden, T.Ohtsubo, A.Ozawa, Z.Patyk, W.R.Plaß, C.Scheidenberger, M.Steck, T.Suzuki, H.Weick, N.Winckler, M.Winkler, T.Yamaguchi, Direct measurement of the 4.6 MeV isomer in stored bare ^{133}Sb

ions, Physics Letters B 688 (2010) 294-297.

7. Tetsuya Ohnishi, Toshiyuki Kubo, Kensuke Kusaka, Atsushi Yoshida, Koichi Yoshida, Masao Ohtake, Naoki Fukuda, Hiroyuki Takeda, Daisuke Kameda, Kanenobu Tanaka, Naohito Inabe, Yoshiyuki Yanagisawa, Yasuyuki Gono, Hiroshi Watanabe, Hideaki Otsu, Hidetada Baba, Takashi Ichihara, Yoshitaka Yamaguchi, Maya Takechi, Shunji Nishimura, Hideki Ueno, Akihiro Yoshimi, Hiroyoshi Sakurai, Tohru Motobayashi, Taro Nakao, Yutaka Mizoi, Masafumi Matsushita, Kazuo Ieki, Nobuyuki Kobayashi, Kana Tanaka, Yosuke Kawada, Naoki Tanaka, Shigeki Deguchi, Yoshiteru Satou, Yosuke Kondo, Takashi Nakamura, Kenta Yoshinaga, Chihiro Ishii, Hideakira Yoshii, Yuki Miyashita, Nobuya Uematsu, Yasutsugu Shiraki, Toshiyuki Sumikama, Junsei Chiba, Eiji Ideguchi, Akito Saito, Takayuki Yamaguchi, Isao Hachiuma, Takeshi Suzuki, Tetsuaki Moriguchi, Akira Ozawa, Takashi Ohtsubo, Michael A. Famiano, Hans Geissel, Anthony S. Nettleton, Oleg B. Tarasov, Daniel P. Bazin, Bradley M. Sherrill, Shashikant L. Manikonda, and Jerry A. Nolen, Identification of 45 New Neutron-Rich Isotopes Produced by In-Flight Fission of a ^{238}U Beam at 345 MeV/nucleon, J. Phys. Soc. Jpn. **79** (2010) 073201.

8. T.Kuboki, T.Ohtsubo, M.Takechi, I.Hachiuma, K.Namihira, T.Suzuki, T.Yamaguchi, Y.Ohkuma, Y.Shimbara, S.Suzuki, R.Watanabe, M.Fukuda, M.Mihara, D.Nishimura, Y.Ishibashi, Y.Ito, T.Moriguchi, D.Nagae, H.Ooishi, K.Ogawa, A.Ozawa, Y.Yasuda, H.Suzuki, T.Sumikama, K.Yoshinaga, H.Geissel, M.Winkler, T.Izumikawa, S.Momota, N.Aoi, N.Fukuda, N.Inabe, D.Kameda, K.Kusaka, T.Kubo, M.Lantz, T.Ohnishi, M.Ohtake, T.Suda, H.Takeda, K.Tanaka, Y.Yanagisawa, A.Yoshida, K.Yoshida, Measurement of Interaction Cross-sections for Neutron-rich Na Isotopes, Acta Phys. Pol. B42, 765 (2011)

9. X.L.Tu, H.S.Xu M.Wang, Y.H.Zhang, Yu.A.Litvinov, Y.Sun, H.Schatz, X.H.Zhou, Y.J.Yuan, J.W.Xia, G.Audi, K.Blaum, C.M.Du, P.Geng, Z.G.Hu, W.X.Huang, S.L.Jin, L.X.Liu, Y.Liu, X.Ma, R.S.Mao, B.Mei, P.Shuai, Z.Y.Sun, H.Suzuki, S.W.Tang, J.S.Wang, S.T.Wang, G.Q.Xiao, X.Xu, T.Yamaguchi, Y.Yamaguchi, X.L.Yan, J.C.Yang, R.P.Ye, Y.D.Zang, H.W.Zhao, T.C.Zhao, X.Y.Zhang, W.L.Zhan
Direct Mass Measurements of Short-Lived A=2 Z-1 Nuclides ^{63}Ge, ^{65}As, ^{67}Se, and ^{71}Kr and Their Impact on Nucleosynthesis in the rp Process, Phys.Rev.Lett. 106, 112501-112505 (2011)

10. N.Aoi, S.Kanno, S.Takeuchi, H.Suzuki, D.Bazin, M.D.Bowen, C.M.Campbell, J.M.Cook, D.-C.Dinca, A.Gade, T.Glasmacher, H.Iwasaki, T.Kubo, K.Kurita, T.Motobayashi, W.F.Mueller, T.Nakamura, H.Sakurai, M.Takashina, J.R.Terry, K.Yoneda, H.Zwahlen, Enhanced collectivity in ^{74}Ni, Phys.Lett. B 692, 302-306 (2010)

11. E.Yu.Nikolskii, A.A.Korsheninnikov, H.Otsu, H.Suzuki, K.Yoneda, H.Baba, K.Yamada, Y.Kondo, N.Aoi, A.S.Denikin, M.S.Golovkov, A.S.Fomichev, S.A.Krupko, M.Kurokawa, E.A.Kuzmin, I.Martel, W.Mittig, T.Motobayashi, T.Nakamura, M.Niikura, S.Nishimura, A.A.Ogloblin, P.Roussel-Chomaz,

A.Sanchez-Benitez, Y.Satou, S.I.Sidorchuk, T.Suda, S.Takeuchi, K.Tanaka, G.M.Ter-Akopian, Y.Togano, M.Yamaguchi, Search for ^{7}H in ^{2}H+^{8}He collisions, Phys.Rev. C 81, 064606-064610 (2010)

12. D. Nagae, T. Ishii, R. Takahashi, M. Asai, H. Makii, A. Osa, T.K. Sato, S. Ichikawa, Y.R. Shimizu, T. Shoji, Lifetime Measurements for the First 2^{+} States in $^{162, 164}$Gd Populated by the Decay of $^{162, 164}$Eu, AIP Conf. Proc., 1224, 156-160 (2010)

13. P.Zhou, D.Q.Fang, Y.G.Ma, X.Z.Cai, J.G.Chen, W.Guo, X.Y.Sun, W.D.Tian, H.W.Wang, G.Q.Zhang, X.G.Cao, Y.Fu, Z.G.Hu, J.S.Wang, M.Wang, Y.Togano, N.Aoi, H.Baba, T.Honda, K.Okada, Y.Hara, K.Ieki, Y.Ishibashi, Y.Itou, N.Iwasa, S.Kanno, T.Kawabata, H.Kimura, Y.Kondo, K.Kurita, M.Kurokawa, T.Moriguchi, H.Murakami, H.Oishi, S.Ota, A.Ozawa, H.Sakurai, S.Shimoura, R.Shioda, E.Takeshita, S.Takeuchi, K.Yamada, Y.Yamada, Y.Yasuda, K.Yoneda, T.Motobayashi, Measurement of two-proton correlation from the break-up of ^{23}Al, International Journal of Modern Physics E, 19 (2010) 957-964

14. D. Nishimura, M. Fukuda, M. Takechi, M. Mihara, D. Ishikawa, J. Komurasaki, K. Matsuta, R. Matsumiya, T. Kuboki, M. Yoshitake, T. Suzuki, T. Yamaguchi, S. Nakajima, K. Saito, M. Miura, I. Hachiuma, K. Namihira, T. Ohtsubo, Y. Shimbara, T. Watanabe, Y. Ohkuma, T. Izumikawa, K. Tanaka, T. Suda, A. Ozawa, Y. Yasuda, T. Moriguchi, S. Momota, S. Fukuda, S. Sato, M. Kanazawa, A. Kitagawa, Distinction between Proton-Neutron Density Distribution of Halo Nuclei at the Nuclear Surface via Reaction Cross Section, Nuclear Physics A 834 (2010) 470c-472c

MATERIALS AND CLUSTER SCIENCE

15. Masashi Imanaka, Shigeo Tomita , Suguru Kanda, Mitsuteru Fujieda, Kimikazu Sasa, Jens Olaf Pepke Pedersen, Hiroshi Kudo, Nanoparticle Formation in H_2O/N_2 and H_2O/Ar Mixtures under Irradiation by 20 MeV Protons and Positive Corona Discharge, Journal of Aerosol Science 41 468–474 (2010).

16. Shaoqiang Chen, Akira Uedono, Shoji Ishibashi, Shigeo Tomita, Hiroshi Kudo, and Katsuhiro Akimoto, Effect of V/III flux ratio on luminescence properties and defect formation of Er-doped GaN, Appl. Phys. Lett. 96, (2010) 051907 (1-3)

17. H. Kudo, H. Arai, S. Tomita, S. Ishii, T. Kaneko, Electron emission from surfaces bombarded by MeV atom clusters, Vacuum 84, (2010) 1014-1017

18. Masashi Imanaka, Shigeo Tomita, Suguru Kanda, Mitsuteru Fujieda, Kimikazu Sasa, Jens Olaf Pepke Pedersen, Hiroshi Kudo, Nanoparticle Formation in H_2O/N_2 and H_2O/Ar Mixtures under Irradiation by 20 MeV Protons and Positive Corona Discharge", J. Aerosol Sci. 41, (2010) 468-474

19. Shaoqiang Chen, Benjamin Dierre, Woong Lee, Takashi Sekiguchi, Shigeo Tomita, Hiroshi Kudo, and Katsuhiro Akimoto, Suppression of concentration quenching of Er-related luminescence in Er-doped GaN, Appl. Phys. Lett. 96, (2010) 181901(1-3)

20. H. Zettergren, H.A.B. Johansson, H.T. Schmidt, J. Jensen, P. Hvelplund, S. Tomita, Y. Wang, F. Martin, M. Alcami, B. Manil, L. Maunoury, B.A. Huber, and H. Cederquist, Magic and hot giant fullerenes formed inside ion irradiated weakly bound C_{60} clusters, J. Chem. Phys. 133, (2010) 104301(1-4)

21. S. Tomita, M. Murakami, N. Sakamoto, S. Ishii, K. Sasa, T. Kaneko, and H. Kudo, Reduction in the energy loss of 0.5 MeV/atom carbon cluster ions in thin carbon foils, Phys. Rev. A 82, (2010) 044901(1-4)

22. Masataka Ohkubo, Shigetomo Shiki, Masahiro Ukibe, Shigeo Tomita, Shigeo Hayakawa, Direct mass analysis of neutral molecules by superconductivity, Int. J. Mass Spectrum. 299, (2011) 94-101

23. M. Minagawa, H. Yanagihara, K. Uwabo, Eiji Kita, K. Mibu, Composition shift as a function of thickness in $Fe_{3-\delta}O_4$(001) epitaxial films, Jpn. J. Appl. Phys., 49 080216-3 page (2010).

24. Eiji Kita, Tatsuya Oda, Takeru Kayano, Suguru Sato, Makoto Minagawa, Hideto Yanagihara,Mikio Kishimoto, Chiharu Mitsumata, Shinji Hashimoto, Keiichi Yamada and Nobuhiro Ohkohchi, Ferromagnetic nanoparticles for magnetic hyperthermia and thermoablation therapy, J. Phys. D: 43, 474011 - 9pages, (2010)

25. M. Minagawa, H. Yanagihara, M. Kishimoto, Synthesis of ε–Fe_xN ($2 \leq x \leq 3$) submicron particles and the diffusion mechanism of nitrogen atoms, Mater. Trans.: 51 No.12 2173-2176, (2010)

26. D. Sekiba, H. Yonemura, S. Ogura, M. Matsumoto, Y. Kitaoka, Y. Yokoyama, H. Matsuzaki, T. Narusawa, K. Fukutani, Development of miro-beam NRA for hydrogen mapping: Observation of fatigue-fractured surface of glassy alloys, Nuclear Instruments and Methods in Physics Research Section B: Beam Interactions with Materials and Atoms, Volume 269 (2011) 627-631.

27. H. Yonemura, Y. Kitaoka, D. Sekiba, H. Matsuzaki, S. Ogura, M. Matsumoto, Y. Iwamura, T. Ito, T. Nausawa, K. Fukutani, Depth profiling of hydrogen under an atmospheric pressure, Nuclear Instruments and Methods in Physics Research Section B: Beam Interactions with Materials and Atoms, Volume 269 (2011) 632-635.

28. K. Okada, S. Kohiki, S. Luo, A. Kohno, T. Tajiri, S. Ishii, D. Sekiba, M. Mitome, F. Shoji, Oxygen annealing for deuterium-doped indium tin oxide thin films, Physica Status Solidi A, 1-5 (2011)/DOI

10.1002/pssa.201026493.

29. K. Okada, S. Kohiki, S. Luo, D. Sekiba, S. Ishii, M. Mitome, A. Kohno, T. Tajiri, F. Shoji, Correlation between resistivity and oxygen vacancy of hydrogen-doped indium thin oxide films, Thin Solid Films 619 (2011) 3557-4561.

30. S. Luo, S. Kohiki, K. Okada, A. Kohno, T. Tajiri, M. Arai, S. Ishii, D. Sekiba, M. Mitome, F. Shoji, Effects of hydrogen in working gas on valence states of oxygen in sputter-deposited indium thin oxide thin films, Applied Materials & Interfaces, 2 (2010) 663-668.

31. J. Oh, T. Kondo, D. Hatake, Y. Iwasaki, Y. Honma, Y. Suda, D. Sekiba, H. Kudo, J. Nakamura, Significant reduction in adsorption energy of CO on platinum clusters on graphite, The Journal of Physical Chemistry Letters, 1 (2010) 463-466.

ACCELERATOR MASS SPECTROMETRY

32. Yoshinori Iizuka, Hideki Miura, Shogo Iwasaki, Hideaki Maemoku, Takanobu Sawagaki, Ralf Greve, Hiroshi Satake, Kimikazu Sasa and Yuki Matsushi, Evidence of past migration of the ice divide between the Shirase and Sôya drainage basins derived from chemical characteristics of the marginal ice in the Sôya drainage basin of East Antarctica, Journal of Glaciology, Volume 56, Number 197 , pp. 395-404, August 2010.

33. Yuki Matsushi, Tsuyoshi Hattanji, Sanae Akiyama, Kimikazu Sasa, Tsutomu Takahashi, Keisuke Sueki, and Yukinori Matsukura, Evolution of solution dolines inferred from cosmogenic ^{36}Cl in calcite, Geology, Vol.38, 11 1039-1042 (2010).

34. Yuki Tosaki, Norio Tase, Kimikazu Sasa, Tsutomu Takahashi, and Yasuo Nagashima, Estimation of groundwater residence time using the ^{36}Cl bomb pulse, Ground Water, doi:10.1111/j.1745-6584.2010.00795.x. (2011).

35. Yuki Tosaki, Norio Tase, Akihiko Kondoh, Kimikazu Sasa, Tsutomu Takahashi and Yasuo Nagashima, Distribution of ^{36}Cl in the Yoro River Basin, Central Japan, and Its Relation to the Residence Time of the Regional Groundwater Flow System, Water, 3, 64-78, 2011.

36. Subash C.B. Gopinatha, Koichi Awazua, Makoto Fujimaki, Penmetcha K.R. Kumarb and Tetsuro Komatsubara, Optimization of silica surface with nanosize holes for immobilization of biomolecules and analysis of their interactions, Analytica Chimica Acta, Volume 680, Issues 1-2, 8 November 2010, Pages 72-78

6.2 International conferences

1. Kimikazu Sasa (Invited talk), Industrial use of accelerator facilities operated by research institutes in Japan, Joint Asian Accelerator Workshop 2010, Pohang, Korea, 29-30 Nov. 2010.

2. K. Sasa, T. Takahashi, Y. Nagashima, Y. Tosaki, N. Kinoshita, K. Sueki, H. Matsumura, K. Bessho, Y. Matsushi, Accelerator mass spectrometry at the tsukuba 12 mv pelletron tandem accelerator, The first International Particle Accelerator Conference(IPAC10), 23rd to 28th, May, 2010, Kyoto International Conference Center (ICC Kyoto).

3. K. Sasa, Y. Matsushi, Y. Tosaki1, T. Takahashi, K. Sueki, N. Kinoshita, K. Kurosumi, T. Amano, J. Kitagawa, K. Horiuchi, H. Matsuzaki and H. Motoyama, ^{36}Cl profiles in the Dome Fuji ice core during the last deglaciation, The Twelfth International Conference on Accelerator Mass Spectrometry (AMS-12), Wellington, New Zealand at the Museum of New Zealand, Te Papa Tongarewa, (Te Papa) on 20 – 25 March 2011.

4. K. Sasa, T. Takahashi, K. Sueki, N. Kinoshita, Y. Tosaki, Y. Matsushi, T. Amano, J. Kitagawa, K. Kurosumi, M. Matsumura, S, Abe, Y, Nagashima, H. Matsumura, Progress on ^{36}Cl AMS with the 12UD Pelletron tandem accelerator at the University of Tsukuba, The Twelfth International Conference on Accelerator Mass Spectrometry (AMS-12), Wellington, New Zealand at the Museum of New Zealand, Te Papa Tongarewa, (Te Papa) on 20 – 25 March 2011.

5. K. Sueki, M. Tamari, T. Amano, J. Kitagawa, K. Sasa, T. Takahashi, Y. Matsushi, Y. Tosaki, K. Kurosumi, Y. Nagashima, N. Kinoshita and H. Matsumura, Isotope ratios of ^{36}Cl/Cl in surface soils at the equal-latitude in Japan, The Twelfth International Conference on Accelerator Mass Spectrometry (AMS-12), Wellington, New Zealand at the Museum of New Zealand, Te Papa Tongarewa, (Te Papa) on 20 – 25 March 2011.

6. J. Kitagawa, T. AmanO, K. Sueki, K. Sasa, T. Takahashi, N. Kinoshita, Y. Matsushi, H.Matsuzaki, Intercomparison study with radionuclides ^{129}I, ^{36}Cl, and ^{137}Cs in soils, The Twelfth International Conference on Accelerator Mass Spectrometry (AMS-12), Wellington, New Zealand at the Museum of New Zealand, Te Papa Tongarewa, (Te Papa) on 20 – 25 March 2011.

7. Kazuna Kurosumi, Kimikazu Sasa, Keisuke Sueki, Tsutomu Takahashi, Norikazu Kinoshita, Takahiro Amano, Junichi Kitagawa, Masumi Matsumura, Yuki Matsushi, Yuki Tosaki, Kazuho Horiuchi, Hiroyuki Matsuzaki, Hideaki Motoyama, A fluctuation of ^{36}Cl depositional flux recorded in an Antarctic ice core: implication to the enhanced cosmic-ray intensity around 11 ka, The Twelfth International Conference on Accelerator Mass Spectrometry (AMS-12), Wellington, New Zealand at

the Museum of New Zealand, Te Papa Tongarewa, (Te Papa) on 20 – 25 March 2011.

8. H. Tsuchida, S. Tomita, K. Nishimura, R. Murakoshi, M. Naitoh, K. Sasa, S. Ishii, and A. Itoh, Energy distribution of MeV-energy atomic and diatomic carbon ions transmitted through a tapered glass capillary, 24th International Conference on Atomic Collisions in Solids (ICACS- 24), Kraków, Poland, July 18-23, 2010.

9. H. Yanagihara, K. Uwabo and E. Kita, Perpendicular magnetic anisotropy in $CoFe_2O_4$(001) films epitaxially grown on MgO(001), 55th Annual Conference on Magnetism and Magnetic Materials, November 14-18, 2010, Atlanta, USA.

10. M. Minagawa, H. Yanagihara, E. Kita, and M. Kishimoto, "Synthesis of γ'-Fe_4N particles by two-step nitridation and the thermal activating processes, The 2nd International Symposium on Advanced Magnetic Materials and Applications (ISAMMA 2010), (Sendai, Japan, July 12-16, 2010) RB-12.

11. Eiji Kita, Ferromagnetic nanoparticles for magnetic hyperthermia and thermoablation therapy (Invited), The 7th International Conference on Fine Particle Magnetism (ICFPM-07), (Uppsala, Sweden, June 21-24, 2010).

12. D. Sekiba, Combinatorial PCT measurement of Mg-Ni hydrogen storage alloy by using ambient micro-beam nuclear reaction analysis, 21st International Conference on the Application of Accelerators in research & Industry (CAARI 2010), August 8-13, 2010, Fort Worth, Texas USA.

13. K. Setoodehnia, A.A. Chen, T. Komatsubara, S. Kubono, D.N. Binh, T. Hahshimoto, T. Hayakawa, Y. Ishibashi. Y. Ito, D. Kahl, T. Moriguchi, H. Ooishi, A. Ozawa, T. Shizuma, Y. Sugiyama, H. Yamaguchi, Study of astrophysically important resonant states in ^{30}S using the $^{28}Si(^{3}He,n\gamma)^{30}S$ reaction, The 11th Symposium on Nuclei in the Cosmos, July 2010, Heidelberg.

7. THESES

Ph. D. thesis

Makoto MINAGAWA	Study on the synthesis and formation process of nano-sized iron oxide and nitride magnetic materials with Mössbauer spectroscopy

Master's theses

Takeru KAYANO	Development of novel magnetic materials for thermo-magnetic cancer therapy
Takuro YOSHIKAWA	Electronic structure of antiferromagnetic FeO synthesized under high pressure
Yoko ISHIBASHI	Production of nuclear polarization of unstable nuclei by polarization transfer reactions
Hiroto OOISHI	Measurements of interaction cross sections of Na isotopes in RIBF
Kazuki SATOU (Waseda Univ.)	Shape recognition of metal nano-films and nanoparticles and detection of heavy metals using waveguide-mode sensors
Takahumi KATO (Waseda Univ.)	Basic research for development of optimal waveguide-mode sensors as high-sensitivity bio-sensors

Undergraduate theses

Satoshi ITO	Measurement of magnetic moment of isomer state of ^{24}Al
Ryo NISHIKIORI	alpha-particle scattering from ^{12}C in 30 MeV
Takahiro NIWA	Developments of solid Ne detectors for detection of RI beams
Toshiyuki YUASA	Angular distribution of γ rays on ^{26}Si for astrophysical implication

Naotsugu TAKEMOTO	Hydrogen determination of a-C:H for solar cell studies by ion-beam analysis
Seigo MIZUNO (Waseda Univ.)	Observation of plating solution using waveguide-mode sensors

8. SEMINARS

2010

1 April — Measurement of azimuthal anisotropy and quark number scaling in Au Au 200GeV at RHIC
Yoshimasa Ikeda (Univ. of Tsukuba)

6 July — Origin of the elements gold and platinum - KISS project –
Hiroari Miyatake (KEK)

2011

12 Jan — Production of nuclear polarization for unstable nuclei via nuclear polarization transfer reaction
Yoko Ishibashi (Univ. of Tsukuba)

Measurement of interaction cross section of Na isotope at RIBF
Hiroto Ooishi (Univ. of Tsukuba)

24 Jan — Research on the interaction of high pt particles with QGP using 2+1 correlation in 200GeV Au+Au collisions at RHIC-PHENIX
Toshimasa Takeuchi (Univ. of Tsukuba)

9. LIST OF PERSONNEL

Tandem Accelerator Complex

E. Kita	Director, Professor
K. Sasa	Assistant Professor
T. Komatsubara	Assistant Professor
D. Sekiba	Assistant Professor
S. Ishii	Mechanical Engineer
H. Kimura	Computer Engineer
H. Oshima	Electric Engineer
Y. Tajima	Mechanical Engineer
T. Takahashi	Electric Engineer
Y. Yamato	Electric Engineer
N. Kinoshita	Research Fellow
Y. Tagishi	Research Supporter
K. Iitake	Administrative Stuff
S. Abe	Administrative Stuff

Research Members[1]

Inst. of Physics

T. Komatsubara	I. Arai	D. Nagae	A. Ozawa
K. Sasa	H. Suzuki		

Inst. of Applied Physics

S. Aoki	K. Akimoto	E. Kita	T. Suemasu
S. Tomita	A. Uedono	H. Yanagihara	D. Sekiba

Inst. of Materials Science

T. Kondo

Inst. of Engineering Mechanics and Systems

K. Matsuuchi

[1]The "research members" include the authors and coauthors within 5 years back from this fiscal year, as well as the members of research projects running at UTTAC.

Inst. of Geoscience

M. Kurosawa N. Tase

Inst. of Chemistry

K. Sueki

Staff of Open Advanced Facilities Initiative

H. Naramoto H. Kudo H. Shen M. Matsumura

H. Muromachi

Graduate students

Doctoral Programs of Pure and Applied Science

M. Minagawa T. Moriguchi K. Yamaguchi Y. Ito

Master's Programs of Pure and Applied Science

K. Oda	Y. Ishibashi	H. Ooishi	K. Yokoyama
Y. Abe	K. Okumura	S. Fukuoka	S. Nakamura
T. Kayano	S. Sato	T. Yoshikawa	T. Amano
J. Kitagawa	K. Kurozumi	T. Nishimura	K. Harada
K. Ito	K. Kurita	Y. Watahiki	Y. Sakaoka
H. Tanikawa	S. Tamura	Y. Narita	

Undergraduates

S. Ito	R. Nishikiori	T. Niwa	T. Yuasa
D. Isaka	N. Takemoto	S. Harada	N. Saito
S. Funada	M. Iura	Ying-Shee Wong	K. Kawase

Scientific Gutests and Fellows

K. Awazu	National Institute of Advanced Industrial Science and Technology
M. Fujimaki	National Institute of Advanced Industrial Science and Technology
K. Nomura	National Institute of Advanced Industrial Science and Technology
T. Kato	Waseda Univ.
K. Sato	Waseda Univ.
A. Izaki	Waseda Univ.
A. Yoshida	Waseda Univ.
S. Mizuno	Waseda Univ.
T. Hayakawa	Japan Atomic Energy Agency
Y. Oura	Tokyo Metropolitan Univ.
Y. Hamanaka	Tokyo Metropolitan Univ.
Y. Sasaki	Tokyo Metropolitan Univ.
S. Yamazaki	Tokyo Metropolitan Univ.
S. Kubono	Center for Nuclear Study, Univ. of Tokyo
S. Cherbini	Catania Univ.
A. A. Chen	McMaster Univ.
K. Setoodehnia	McMaster Univ.
J. Chen	McMaster Univ.
H. Tsuchida	Kyoto Univ.
K. Nishimura	Kyoto Univ.
R. Murakoshi	Kyoto Univ.
T. Nagatomo	International Christian Univ.
Y. Hirose	Univ. of Tokyo
S. Mohri	Univ. of Tokyo
D. Oka	Univ. of Tokyo
Y. Tosaki	National Institute of Advanced Industrial Science and Technology
K. Sagara	Kyushu Univ.
S. Kuroita	Kyushu Univ.
T. Yabe	Kyushu Univ.
K. Ishibashi	Kyushu Univ.
T. Tamura	Kyushu Univ.
M. Okamoto	Kyushu Univ.
Y. Maeda	Miyazaki Univ.
A. S. Demyanova	Kurchatov Institute, Russia
A. N. Danilov	Kurchatov Institute, Russia
A. A. Ogloblin	Kurchatov Institute, Russia
N. Saduev	Institute of Nuclear Physics, Kazakhstan